

Postglacial Uplift: Record in the Gravity Field and in Neogene–Quaternary Structures

N.L. Dobretsov^{a,b,✉}, A.N. Vasilevskiy^{a,b}

^a*A.A. Trofimuk Institute of Petroleum Geology and Geophysics, Siberian Branch of the Russian Academy of Sciences,
pr. Akademika Koptyuga 3, Novosibirsk, 630090, Russia*

^b*Novosibirsk State University, ul. Pirogova 2, Novosibirsk, 630090, Russia*

Received 25 December 2018; received in revised form 1 May 2019; accepted 22 May 2019

Abstract—The history of Quaternary glaciation and postglacial uplift in Fennoscandia is considered in relation to the surface topography, gravity, and number of glacial deposits and is compared to the respective processes in North America. The surface topography and the gravity field are correlated over the Fennoscandian region as a whole and for two reference areas of South Norway and the Kola Peninsula. The gravity field is composed as free-air and Bouguer gravity anomalies using modern global models based on satellite data. The impact of glaciation may be responsible for zoned patterns of both topography and gravity. The glaciation centers of Norway are marked by uplifts reaching 2470 and 1500 m and by circular Bouguer gravity lows of ≤ -200 mGal, which correspond to residual crust thickening. The gravity patterns of the Kola Peninsula and Norway consist of circular and polygonal anomalies caused by both postglacial rebound and rock density variations. The general uplift and related extension of the crust led to the formation of fractures of different sizes, from 100–200 km long and 1–2 km deep fjords in Norway to 1–2 km long and 30–20 m deep local fractures on the Kola Peninsula. The gravity field of central North America is characterized by a generalized map of free-air anomalies within the limits of glaciation and a map of free-air anomalies compiled from the global database. Glaciation and its records in the surface topography and gravity patterns are described in more detail for Wisconsin State (USA), where extension fractures are similar to those on the Kola Peninsula. The models explaining the correlation between postglacial uplift and gravity variations can be further updated using seismic and tectonic data, as it was shown previously for the case of Finland.

Keywords: tectonics, geodynamics, postglacial uplift, free-air and Bouguer gravity anomalies, integrated interpretation

INTRODUCTION

Late Quaternary glaciation produced large 3–5 km thick ice sheets in northern Europe and Asia, as well as on the Canadian shield, which are similar to the present Greenland or Antarctica ice sheets (Kotlyakov and Lorius, 2000; Kotlyakov et al., 2004). The best known are the Fennoscandian, Kara, and Canadian ice sheets that formed between 150 and 90 kyr BP. Large ice sheets reappeared in these areas also during the Last Glacial event, 25–12 kyr BP, though the Fennoscandian one was smaller than its older precursor (Mörner, 1969; Kukkamaki, 1975; Grossvald, 1999; Svendsen et al., 2004).

Deglaciation in Fennoscandia at 9–12 kyr BP induced uplift of the territory, which still continues. The uplift was attributed to the presence of asthenosphere beneath the continent, and the asthenospheric viscosity was estimated via the uplift rate (Niskanen, 1939; Artyushkov, 1967, 1971,

1979; Mörner, 1969, 1980; Tolkunova, 1977; Zharkov, 1983; Lidberg et al., 2010).

Advanced satellite altimetry facilities have furnished high-resolution gravity data for both continental and oceanic areas (Andersen and Knudsen, 2016). Recently interest has been rekindled to Late Neogene uplifts, of which some originated otherwise than by postglacial isostatic rebound (Artyushkov et al., 2018), as well as to Neogene–Quaternary uplifts in the Kola Peninsula (Nikolaeva et al., 2018), Norway, and Sweden (Mörner, 2004; Ojala et al., 2004; Simon et al., 2018). It is also interesting to study the uplift that followed the 15–17 kyr BP Quaternary glaciation in Wisconsin (USA). It was the visit of one of us (N.L.D.) to the Wisconsin area in May 2018 that inspired this study.

New high-resolution gravity data can provide insights into the deep structure of areas covered by present (Greenland and Antarctica) or past (Fennoscandia, etc.) ice sheets, and especially the areas of postglacial uplift. The objective of this paper is to compare gravity maps with the distribution of Neogene–Quaternary structures produced by postglacial crust movements in Fennoscandia (including the

✉ Corresponding author.

E-mail adress: DobretsovNL@ipgg.sbras.ru (N.L. Dobretsov)

Kola Peninsula) and in the Canadian shield (Wisconsin and its surroundings), and to discriminate between upper crustal and deeper features.

SURFACE TOPOGRAPHY, NEOGEN–QUATERNARY STRUCTURES, AND GRAVITY MAPS OF FENNOSCANDIA

Figure 1 shows reconstructed limits and history of the Fennoscandian and Kara ice sheets from 150 through 20 kyr BP (Grosswald, 1999; Svendsen et al., 2004). The data on postglacial Fennoscandia are presented Fig. 2: reconstructed uplift to 800 m (Ojala et al., 2004) and its deviation from average uplift in panel *a*; deviations of uplift from the calculated isostatic values, negative in panel *b* and positive in *c*; and current vertical and horizontal velocities according to GPS in panel *d* (Lidberg et al., 2010). Additionally, we have revealed local uplift peaks (panel *a*) which were first outlined by Artyushkov (1979) who mentioned that general uplift in central Fennoscandia had stopped around 9000 yr BP, and the area underwent uplift and subsidence of different blocks since then. That inference was confirmed by many later models (Stewart et al., 2000; Siegert et al., 2001; Simon et al., 2018).

An axis of local uplifts across the South and North Norwegian maximums (Figs. 1, 2) roughly coincides with that of maximum ice thickness that reached 2.5–3.0 km (Grosswald, 1999; Siegert et al., 2001), whereas the maximum present uplift is shifted southward (Fig. 2). Another axis traverses uplifts 3–5 (Figs. 1, 2*a*). The current uplift rate (Fig. 2*d*) of 1.6 cm/yr (Ojala et al., 2004; Lidberg et al., 2010) is slower than 3–4 cm/yr at 9–10 kyr BP and 10–12 cm/yr about 11.5 kyr BP: it became 3 to 5 times slower for 1500 yr, and the total reduction has been by a factor of 7–8 (Artyushkov, 1979). The axes of maximum uplift and Bouguer gravity lows better highlight the northern line and the northern local zones of thick crust (see below). Thus, the uplift rate was decreasing exponentially with time for 10–12 kyr while the maximum has shifted from southern Norway northeastward to the northern Gulf of Bothnia.

Southwestern Fennoscandia (Norway and the adjacent part of Sweden), with its high mountains and deep fjords (blue areas in Fig. 3), stands out in the shadow relief model based on the DTU15 global model (Andersen and Knudsen, 2016) that covers also the surrounding offshore and East European craton areas (Fig. 3). Tectonically, it is a zone of Norwegian Caledonides (Yanshin, 1966) with the thickest

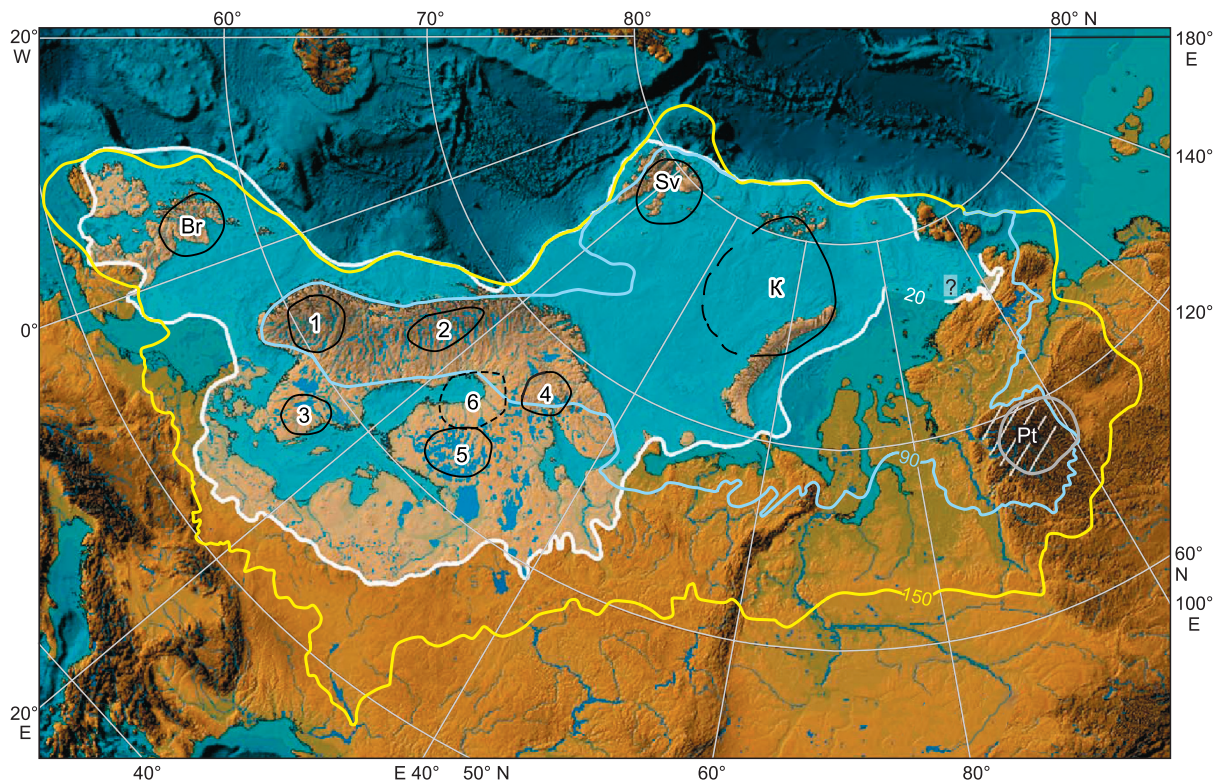


Fig. 1. Reconstructions of the Fennoscandian and Kara ice sheets, ca. 150–20 kyr BP (Grosswald, 1999; Svendsen et al., 2004). Limits of the Barents–Kara ice sheet (extended version) are according to (Landvik et al., 1998; Svendsen et al., 2004). White, blue, and yellow lines: glacial limits in Europe and the glacialiation peak in Norway and Sweden at 20, 90 and 150 kyr BP, respectively (Grosswald, 1999; Ehlers and Gibbard, 2004). Valley glaciers in the Alps, Iceland, and other mountain systems are not shown. White hatching: remnant glaciers at the Putorana Plateau. Letters in circles are names of glacialiation centers, abbreviated as: Br, British; Sv, Svalbard; K, Kara–Barents Sea; Pt, Putorana Plateau. Ovals with numerals from 1 through 6 are zones of maximum uplift, numbered as in Fig. 2*a*.

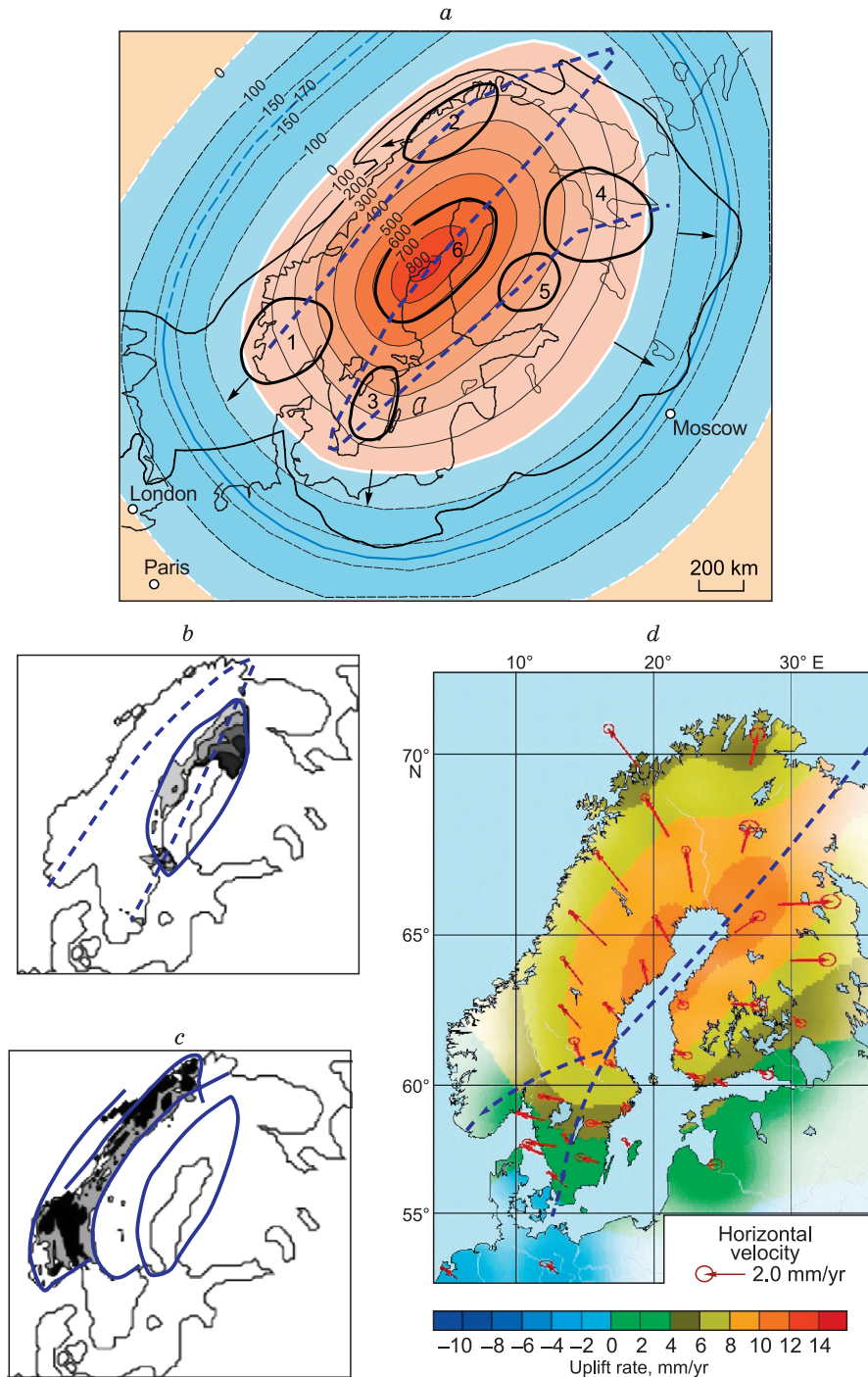


Fig. 2. *a*: Total uplift (m) in Fennoscandia, complemented after Simon et al. (2018). Thin black line shows glaciation limits during the last glacial maximum (Mörner, 1980); deviation of this line from averaged symmetrical patterns of uplifts records local uplift at early stages (ca. 9 kyr, zones 1 and 2), intermediate uplift (4000 yr, zones 3, 4 and 5), and the present maximum uplift (zone 6); *b* and *c*: maximum negative deviation from averaged pattern, where uplift is overestimated (*b*) and positive deviation where it is underestimated (*c*) with respect to calculated isostatic uplift (Fjeldskaar et al., 2000; Ojala et al., 2004); blue solid lines: contours of the deviation zones; *d*: horizontal velocities based on GPS data (red arrows, 95% confidence ellipse); color scale shows rates of subsidence and uplift (see text).

crust (Nikolaev, 1979; Artemieva and Thybo, 2013; Maupin et al., 2013).

In the continental part, the transition zone adjacent to the uplift axis, which corresponds to the East European craton

margin, encompasses Sweden (except its southwesternmost part), Northern Finland, and the Kola Peninsula. It has generally lower elevations but still high topographic contrasts; in many places it preserves a mosaic crustal pattern clearly

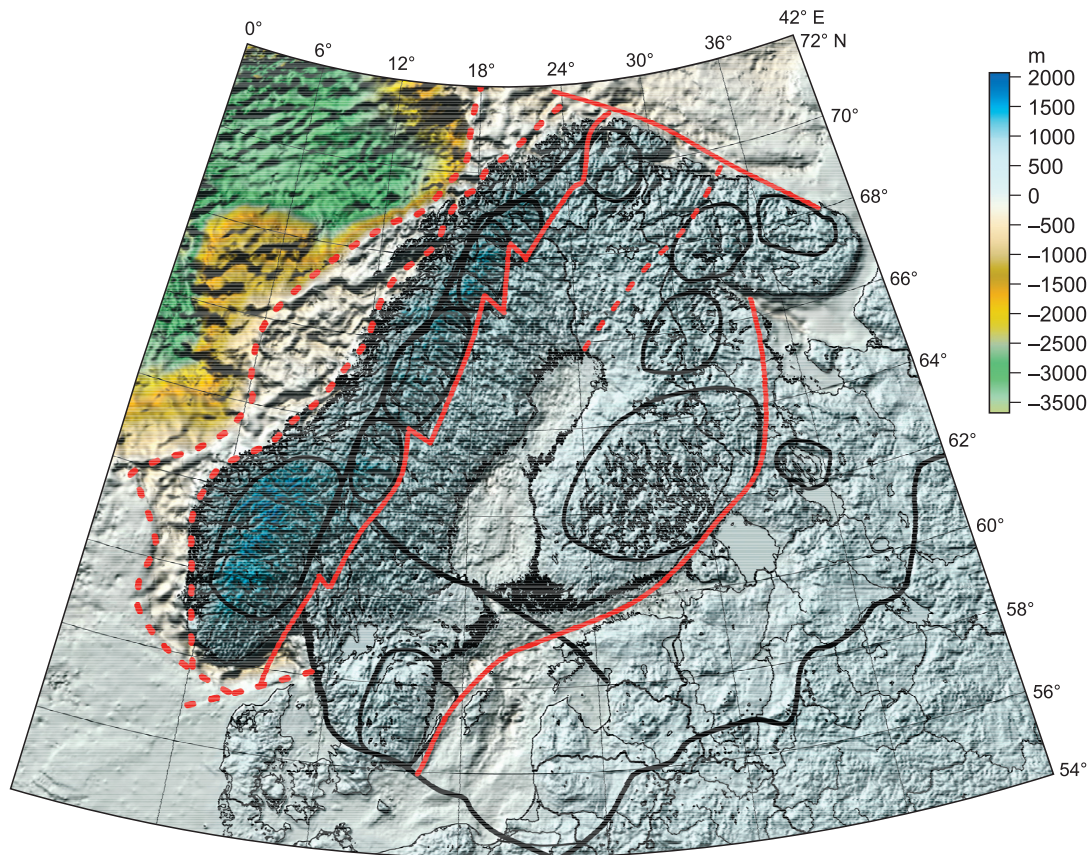


Fig. 3. Shadow relief model of Fennoscandia, a part of the East European craton, and offshore area. Gray, blue, and light blue lines: different heights of postglacial uplift; whitish color: coast and shallow shelf; brown and green: continental slope and oceanic uplift; red lines: maximum axial uplift (peak in South Norway (blue) and its surroundings) and boundaries of the second transition zone in the craton with local uplifts (black ovals); black line: limits of maximum glaciation.

seen in the remaining craton part. The offshore transition zone includes continental shelf with the same mosaic structure and prominent topographic features: light-colored zone in Fig. 3 adjacent to Norway and grading seaward into a yellow-green zone corresponding to old oceanic crust involved into postglacial movements. Another transition zone on the craton comprises four or five circular uplifts with high elevation contrasts and numerous lakes, mostly of glacial origin as generally in Fennoscandia. The uplifts include the largest one located in South Finland and Karelia next to the northwestern edge of Lake Ladoga, and smaller uplifts north and east of it and in South Sweden.

The remaining part of the East European craton (right bottom corner in Fig. 3) comprises a few circular uplifts superposed upon a polygonal fault pattern that corresponds to the old deformation framework inherited by the postglacial fault-bounded uplifts and other structures. The area is divided into two zones separated by a chain of terminal moraines formed during the Last Glacial, which left imprint in the surface topography as moraine landforms and numerous small lakes along the southern margin of the 20 kyr BP ice sheet (Figs. 1, 3). This boundary and the landforms that mark the limits of the thickest ice coincide with the zone of

highest uplift and deformation, which confirms the reliability of the reconstructions in Figs. 1 and 2.

The gravity field of the region was imaged by mapping Faye (free-air) (Fig. 4) and Bouguer (Fig. 5) gravity anomalies with reference to the DTU15 (Andersen and Knudsen, 2016) and EIGEN-6C4 (Förste et al., 2014) global models, respectively. The Bouguer gravity provides important check of the free-air anomalies that are affected by terrain. The Bouguer gravity anomalies were calculated using calculation service and data which available at the ICGEM website (<http://icgem.gfz-potsdam.de/home>), with terrain correction assuming 2.67 g/cm^3 density of rocks. The correction remains incomplete if the real rock density differs from the assumed value, but the upper crust density misfit for Fennoscandia is within $\pm 0.17 \text{ g/cm}^3$ (Olesen et al., 2002; Glaznev et al., 2015), which makes a contribution of $< 7 \text{ mGal}$ per 1000 m of elevation. Therefore, any gravity anomaly above this value must be due to density heterogeneity, with its depth extent exceeding the elevation difference. The regional Bouguer anomalies thus represent deep structures, partly the Moho topography.

The Bouguer gravity map (Fig. 5) images the upper continental lithosphere and the polygonal mosaic pattern of

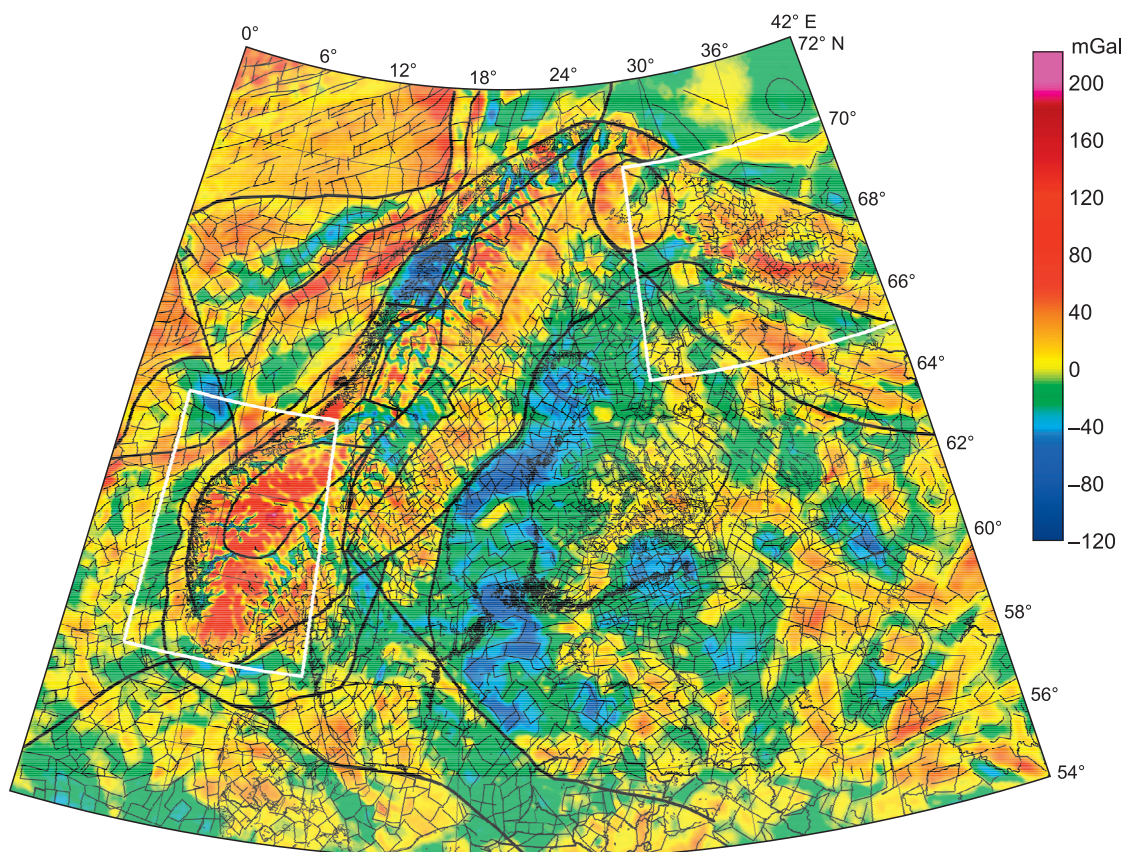


Fig. 4. Free-air gravity anomalies in the area of Fig. 3, based on the DTU15 global model (Andersen and Knudsen, 2016). Heavy black lines: fault boundaries and boundaries of zones with different gravity patterns; thin lines: polygonal mosaic pattern recorded in the gravity field; white boxes are areas enlarged in Figs. 6–9, 11, and 13–15.

postglacial uplift resulting from different uplift rates associated with density variations. The gravity anomalies also record the lower crust and Moho features with oval zones of thick crust (Gradmann and Ebbing, 2015). The crustal features may be isostatically imbalanced (Gradmann and Ebbing, 2015) and, correspondingly, may represent zones of fastest early postglacial uplift in the territory of Norway (Fig. 5). Furthermore, they may be responsible for the mosaic pattern of the remaining craton part (thin lines between local positive and negative anomalies in Figs. 4 and 5). The thin lines make up a regular network of geometrically different elements. In many cases, the lines were drawn with reference to the adjacent patterns to reduce uncertainty caused by low gravity field gradients. The elements of the mosaic structure in the free-air and Bouguer gravity fields differ mainly because they may be ambiguously contoured and because the free-air anomalies bear much larger terrain effects than the Bouguer anomalies. These problems were investigated in more detail for the cases of the Kola Peninsula and South Norway areas (Figs. 4, 5), where the block boundaries were traced using jointly analyzed free-air and Bouguer anomalies and digital terrain maps compiled using function of 2D Laplacian, which are obtained by means of the second derivatives estimation to measure surface curvature. The

function of 2D Laplace of terrain elevations (Dobretsov and Vasilevskiy, 2018) was normalized to the highest value over the study region.

The Bouguer gravity pattern (Fig. 5) includes prominent lows of -90 to -160 mGal in the zone of highest elevations which covers the Norwegian Caledonides and the adjacent part of the East European craton. Smaller gravity lows (< -80 mGal) appear in the southern and central Gulf of Bothnia and near the Kandalaksha Gulf where they make up a wide belt of 0 to -30 mGal features between 59° and 70° N. In the northern end of the belt, near the Murmansk fjord, there is a -40 mGal low surrounded by highs up to $+120$ mGal. A similar feature in Wisconsin and Michigan (USA) is beyond the surface topography zones (Fig. 3), because the Bouguer anomalies bear only a minor surface terrain effect but mostly record lower crustal and Moho heterogeneities, as well as the lithospheric mantle variations. This fact explains partly the scale difference of the free-air and Bouguer anomalies.

Prominent Bouguer gravity lows in the zone of Norwegian Caledonides (Fig. 5) correspond to areas of the thickest granitic crust and generally correlate with the most contrasting surface topography and roots of collisional uplifts (Alps, etc.). However, the collisional crust thickening occurred

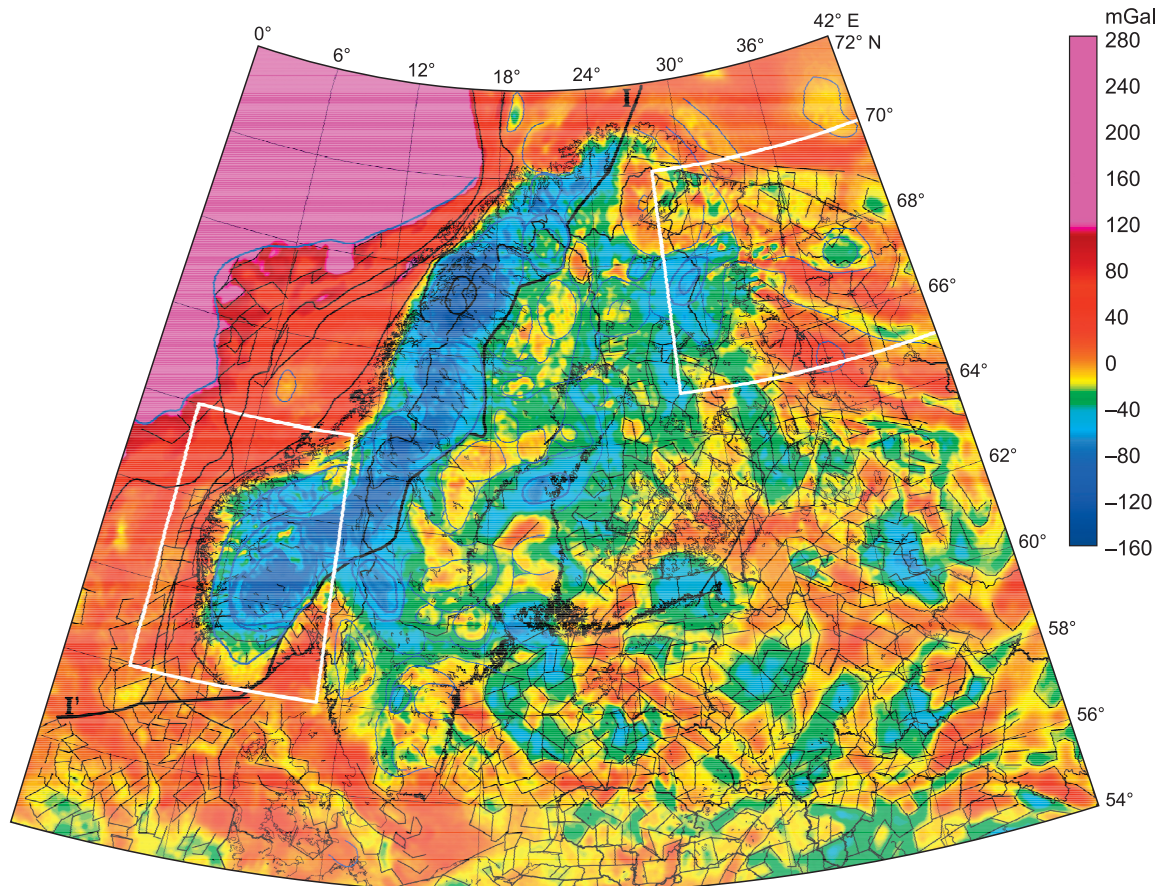


Fig. 5. Bouguer gravity anomalies in the area of Figs. 3 and 4 based on the EIGEN-6C4 global model (Förste et al., 2014). Thin blue lines: gravity lows in the area of maximum uplift in the transitional zone; thin black lines: polygonal mosaic pattern of offshore and cratonic blocks; line I–I': boundary of most intense gravity lows.

most likely in the Devonian and only a part of the thick crust survived till the Cenozoic, e.g., beneath the Ural Late Paleozoic–Early Mesozoic or Kazakhstan Early Paleozoic orogenic structures. The ~3 km thick ice loaded the zones of lighter thick crust, and the most deeply pressed areas uplifted most rapidly by isostatic rebound after ice melting, first at 10–12 cm/yr about 11 kyr BP and then at 2–4 cm/yr about 9 kyr BP, while the present uplift has been 1.6 cm/yr (Fig. 2d) (Artyushkov, 1979; Ojala et al., 2004; Lidberg et al., 2010; Simon et al., 2018).

The magnitude and geometry of gravity lows do not match perfectly the topographic features. The South Norway anomaly is similar in shape to the oval zone of high elevation but the highest mountain (Galdhøpiggen, ~2470 m) falls on the anomaly margin, while the most prominent round Bouguer anomaly coincides with a small uplift centered at Mt. Kebnekaise (2117 m), which is 350 m lower. The uplift within 850 m (Fig. 2a) or 2000 m (?) is about ten times as high as the previously calculated values of 200–250 m (Artyushkov, 1979) that may represent the latest stage of the mountain growth event (past 3 kyr).

The transition zone between the gravity lows of Norway and the flat part of the East European craton encompasses several oval and angular features (Fig. 5). The Bouguer gravity field in the remaining craton part, free from uplifts, has a mosaic pattern similar to that observed in the map of free-air anomalies (Fig. 4), but with smaller-scale structures. Nevertheless, moderate Bouguer gravity lows (within -60 mGal) in this area are square or rhombic (in the contour line map), with high angles, which are similar to gravity highs of $\leq +60$ mGal corresponding to angular blocks of different densities. This pattern may record a larger-scale mosaic structure of the lower crust. The free-air and Bouguer anomalies generally agree in contours and sign but differ in magnitude and surface area (the Bouguer highs are markedly larger and the lows are smaller than the respective free-air features), possibly, as a result of difference between blocks of the lower and upper crust evident in many seismic sections.

The general trends revealed for the large region of Fennoscandia and its surroundings (Figs. 3–5) require further checks and updates for specific key areas. We have chosen South Norway and the Kola Peninsula as examples of highest uplift and transition areas.

DETAILED STRUCTURE AND CORRELATIONS: SOUTH NORWAY AND KOLA PENINSULA KEY AREAS

South Norway (58° to 64° N and 3° to 11° E, Figs. 6–9).

The gravity and surface topography records were compared using a specially created universal system of block boundaries outlined with reference to the maps of transformed (2D Laplacian) elevations (Dobretsov and Vasilevskiy, 2018). The land and sea bottom topography (Fig. 6) maps are based on the DTU15 model (Andersen and Knudsen, 2016) and have a 1" × 1" (~1.8 km × 0.9 km) resolution. The most highly elevated blocks (>2000 m) contoured by ovals are well pronounced.

The dome-shaped oval uplift, around 210 km in radius, centered at Mt. Galdhøpiggen, ~2470 m (white triangle, point 1, in Fig. 6) is the principal topographic feature in this part of Fennoscandia. It is composed of brick-like polygonal blocks with deep incisions of steep-sided and flat-bottomed fjords. The largest Sognefjord is cut 204 km into the land as far as the foot of Mt. Galdhøpiggen and rises 1310 m above the water. The uplift is a series of several concentric ovals with a total length of 600 km between 58° and 63° N and is 350 km wide (Fig. 6). Taking into account the amount of erosion and sediments accumulated on the fjord bottom, the “bricks” can be assumed to be at least 1.5–2.0 km thick. The blocks are smaller (~6 km × 4 km × 1.5 km) in the center of the uplift but 4–5 times larger (up to 30 km × 15 km × 2 km) near the coast. The primary block boundaries are masked by talus and corrom material, while denudation is commonly minor in the high latitudes, and its role has to be further investigated. On the continental slope, large (40 km × 20 km or 30 km × 20 km) blocks have more distinct boundaries while smaller ones may be buried under soft sediments.

The structures with characteristic sizes of small gravity anomalies are better detectable in the map of transformed (2D Laplacian) elevations (Fig. 7), which can highlight terrain features against high elevation gradients and bring out block boundaries that fit both topographic and gravity patterns in zones of low horizontal gradients of gravity.

The division of the South Norway area into small blocks, which appear in the surface topography (Figs. 6, 7), is also evident in the map of free-air gravity anomalies (Fig. 8). In the continental area, the block boundaries are sharp and straight, but the oval features are less prominent, except for their periphery and some ovals in the most highly elevated central part (Fig. 8). The blocks are homogeneous or weakly zoned (<10 mGal). The gradients of local anomalies produced by lateral density variations are especially high along the block boundaries over most of the perimeter.

In shallow shelf, outside the continent, the gravity field is more homogeneous, mostly in the range from 0 to –30 mGal (Fig. 8), with elongated highs up to +60 mGal in the northwest of the area and weaker highs in the southwest (Fig. 8). This gravity distribution differs from the mosaic pattern of surface topography persistent also offshore to 3° E (Figs. 6, 7).

In general, the free-air gravity features become less contrasting and larger toward the uplift periphery, especially, offshore where the blocks are as large as 40 km × 30 km. Their boundaries are obscured by soft sediments, which makes it difficult to decipher the gravity record in hard rocks.

The Bouguer gravity map (Fig. 9) shows two well pronounced concentric radiating negative anomalies decaying from –100 to –120 mGal at the center to –40 to –60 mGal (blue) and then 0 to –40 mGal (yellow-green). Anomaly 1 is located in the center of the southern half of the peninsula and anomaly 2 is farther northeast, about 62° N (partly shown in Fig. 9). The two anomalies are as large as 200 km across and represent structures at the crustal base and coexist with smaller oval and concentric anomalies of some other origin in the transition zone. Northwest of the two features, there is anomaly 3 of a complex “breccia”-like structure, with –90 to –30 mGal values radiating from two centers.

The three Bouguer anomalies (Fig. 9) correlate in different ways with the free-air anomalies (Fig. 8): the southeastern part of Bouguer anomaly 1 and almost whole anomaly 2 match free-air gravity lows (Fig. 8), whereas the northwestern part of anomaly 2 and almost entire anomaly 3 correspond to +30 to +130 mGal free-air anomalies (Fig. 7). The latter highs are in inverse correlation with the –100 to –120 mGal Bouguer lows, which may result from crust thickness difference exceeding 10 km (Artemieva and Thybo, 2013; Maupin et al., 2013; Gradmann and Ebbing, 2015) or from mantle structure difference if the crust thickness is more uniform (Gradmann and Ebbing, 2015). Line I–I' between these zones (Figs. 8 and 9) is tentative.

The plots of filtered terrain elevations presented together with the free-air and Bouguer anomalies along profile A–A' (Fig. 10, top panel; profile location is shown in Figs. 6–9 for) demonstrate the terrain effect on local gravity anomalies. The topography curve (white line) fits perfectly the free-air gravity variations, and many local free-air gravity features correlate with Bouguer anomalies. As noted previously, all local features above 7 mGal must be due to density variations over depths exceeding local elevation difference. The local Bouguer anomalies that correlate with elevation variations may likewise result from density contrasts. The latter may be due either to nonuniform vertical motions of blocks, which brought rocks of different densities to the same hypsometric level or to faster or slower subsidence and uplift of blocks with different densities. The Bouguer gravity curve bends smoothly at 50–100 mGal (Fig. 10), which records the compensation effect of the uplift of roots.

The seismicity of Fennoscandia is concentrated in three roughly parallel belts running along the continental margin boundary in the North Sea, the North Sea coast, and the western side of the Gulf of Bothnia. The two former ones correlate with zones of high crust thickness gradients while the third one falls within the zone of maximum postglacial uplift (Redfield and Osmundsen, 2015).

Kola Peninsula (southern limit at 65° N and western limit at 28° E, Fig. 11a).

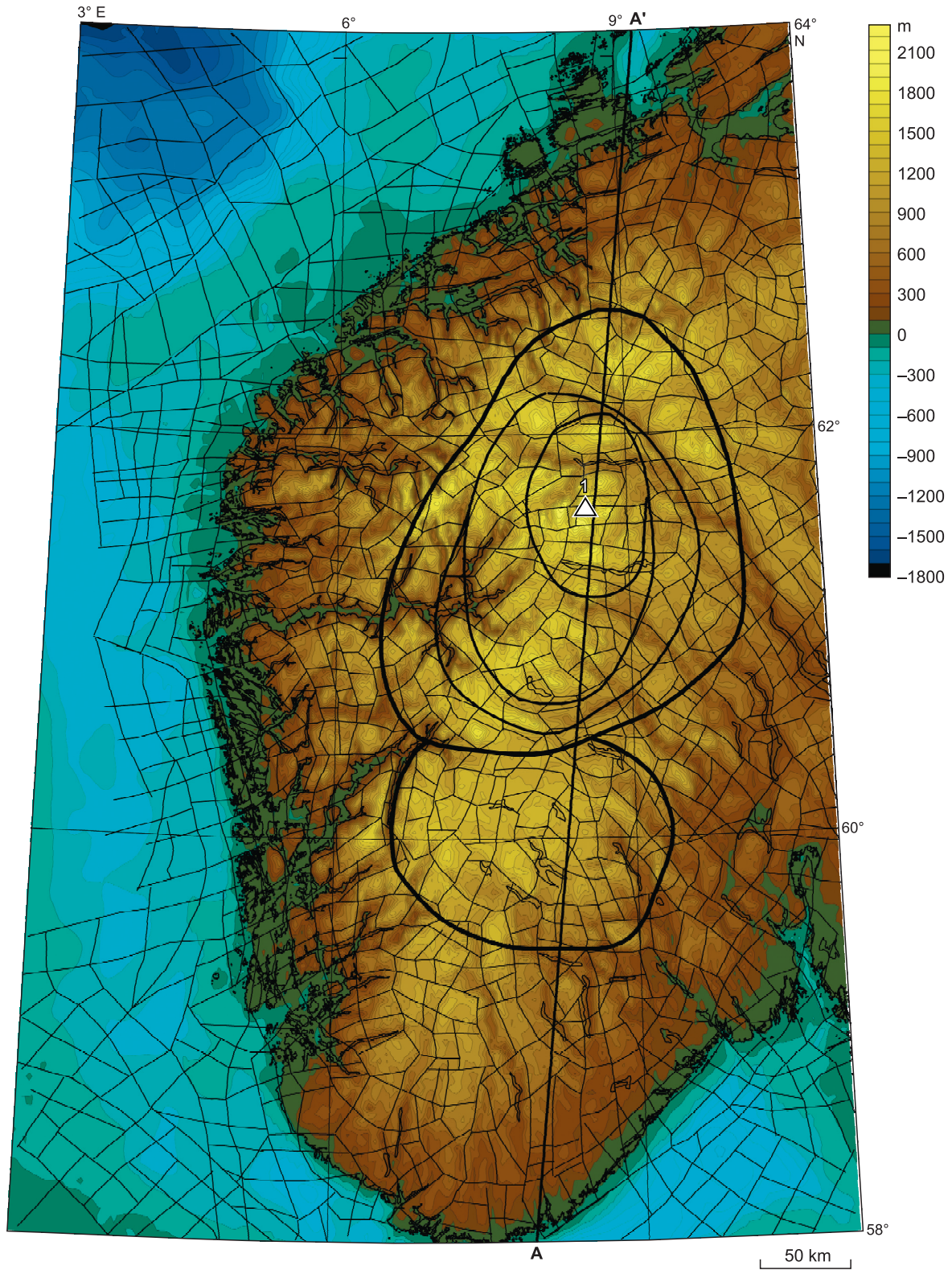


Fig. 6. Surface topography of South Norway. Thin lines: reconstructed polygonal mosaic pattern. Point 1: elevation 2470 m; ovals contour several main uplifts; line A–A' is profile presented in Fig. 10.

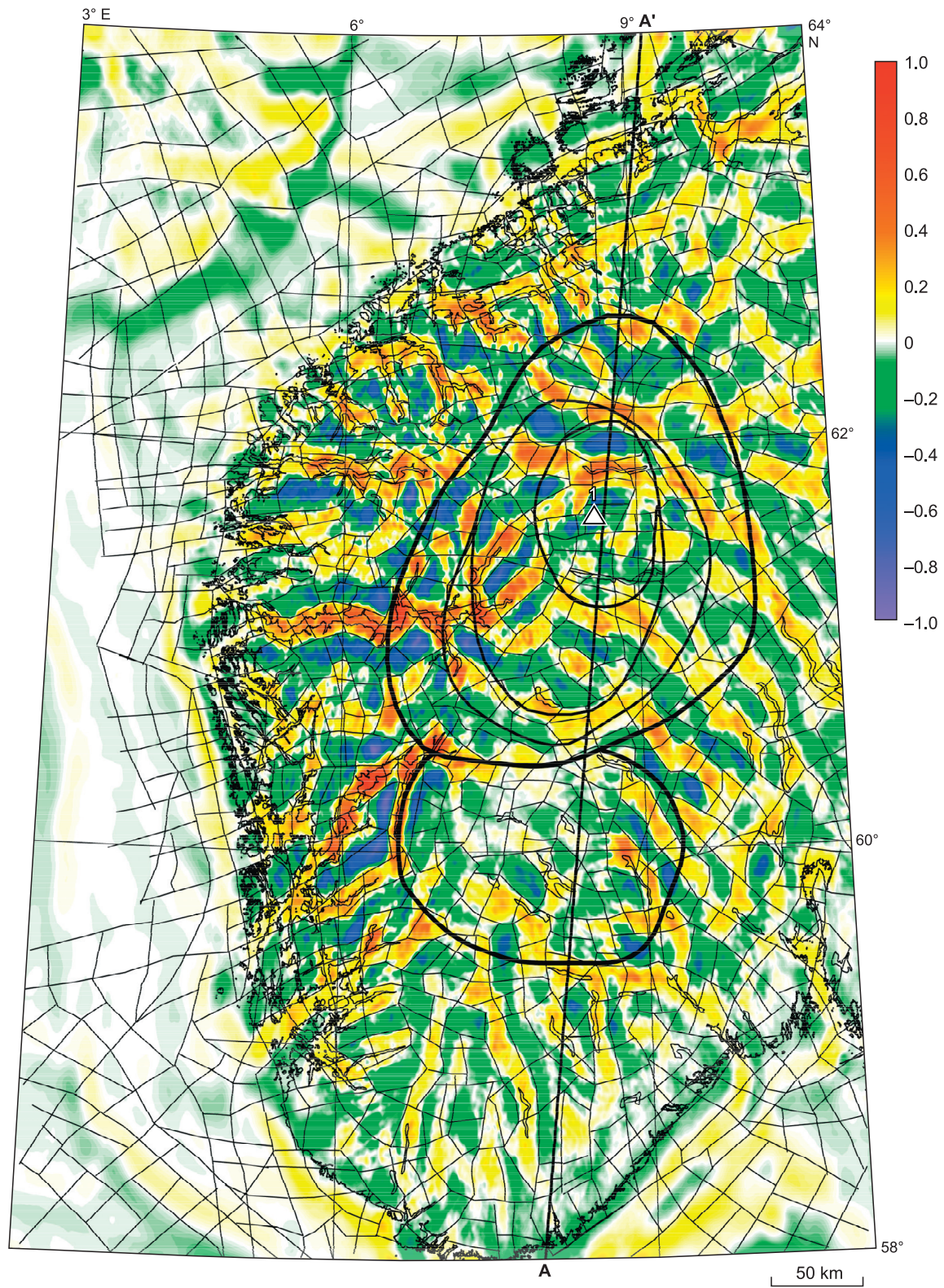


Fig. 7. Transformed surface topography of South Norway (2D Laplacian of terrain elevations normalized to maximum value over the whole area).

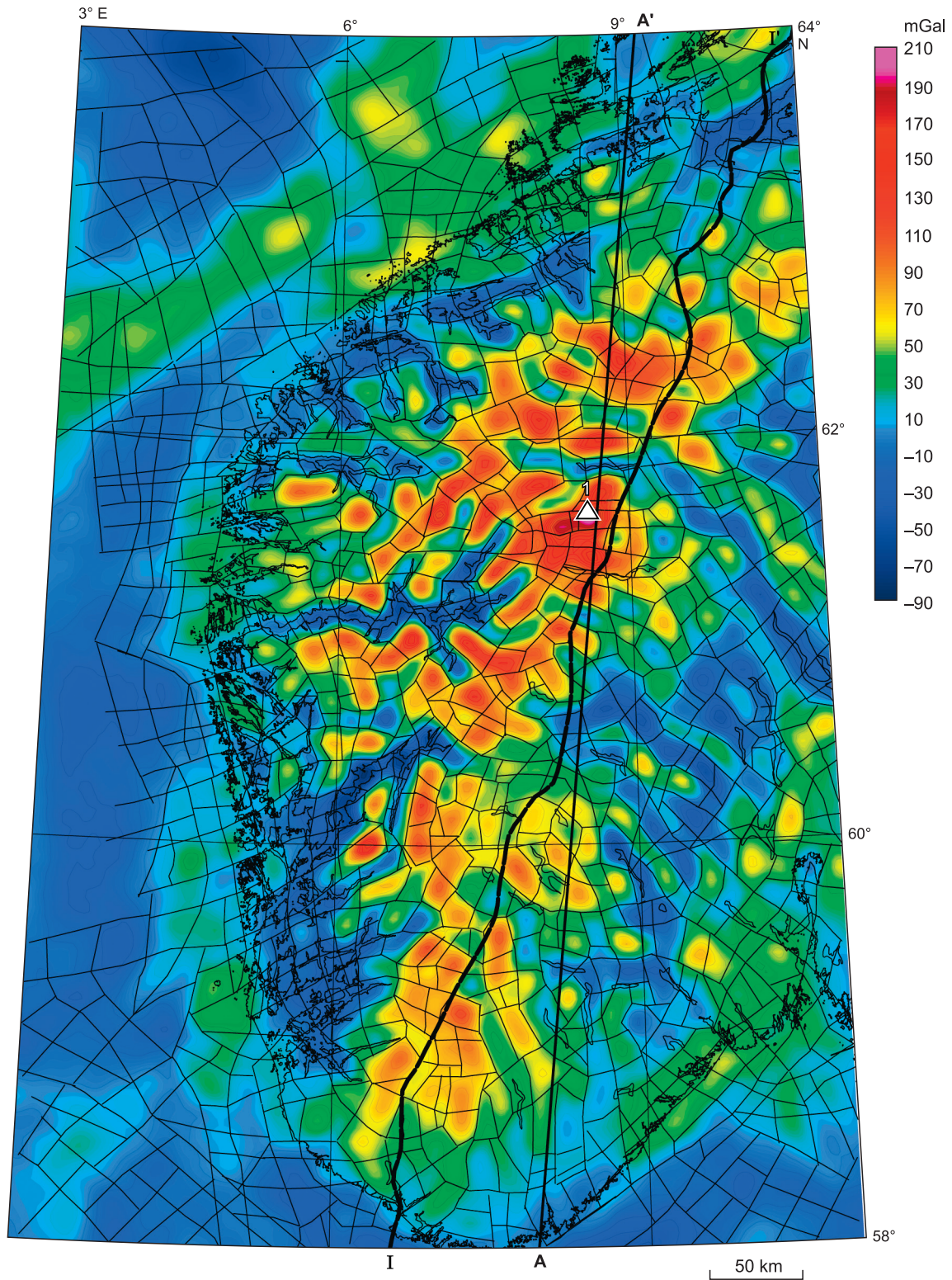


Fig. 8. Free-air gravity anomalies in South Norway and surrounding seas based on DTU15 global model (Andersen and Knudsen, 2016). Thin lines: block boundaries; line I–I': tentative boundaries between different mantle zones at moderate variations in crust thickness. Line A–A' is profile presented in Fig. 10.

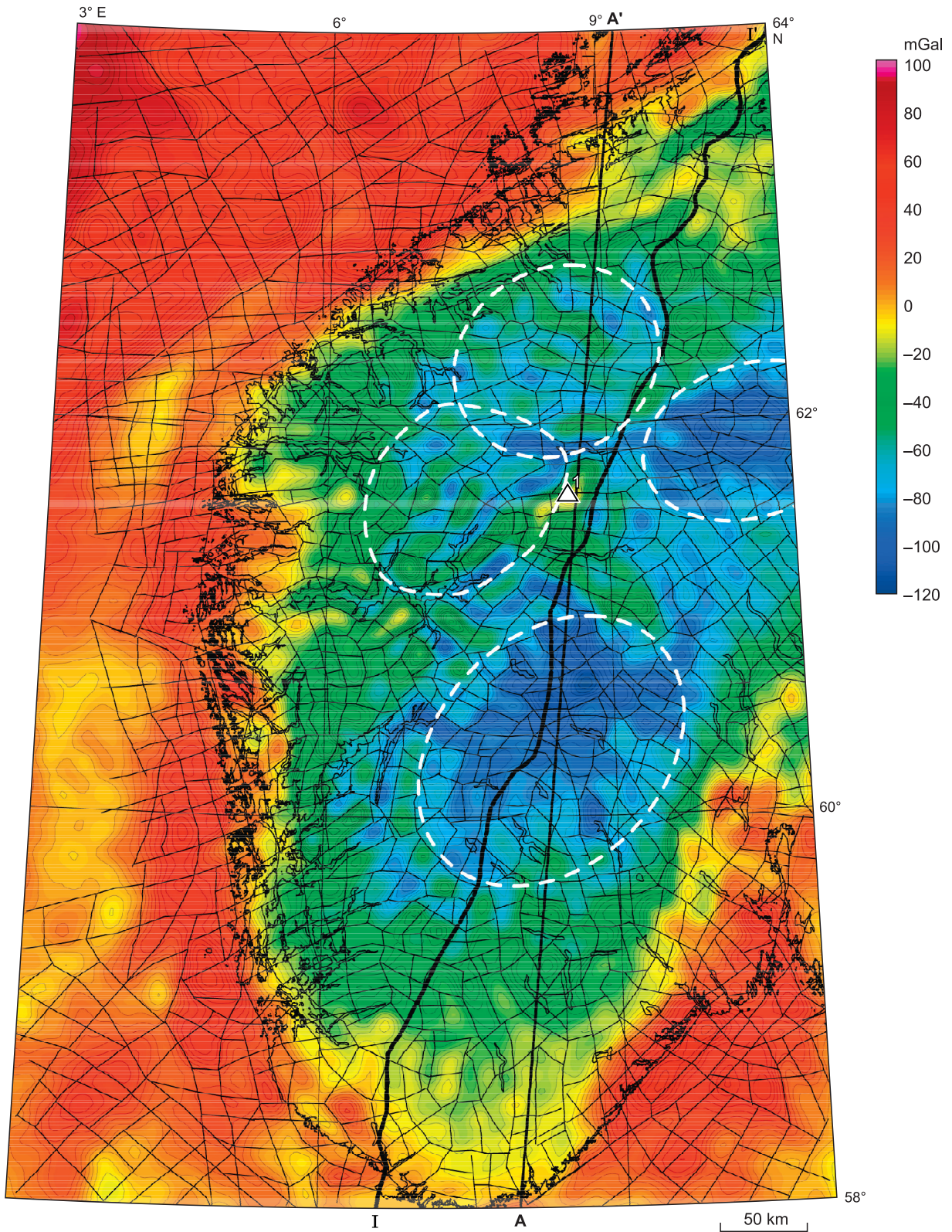


Fig. 9. Bouguer gravity anomalies in South Norway. Thin lines: reconstructed polygonal mosaic pattern. White dash line: oval structures. I-I' is same as in Fig. 8.

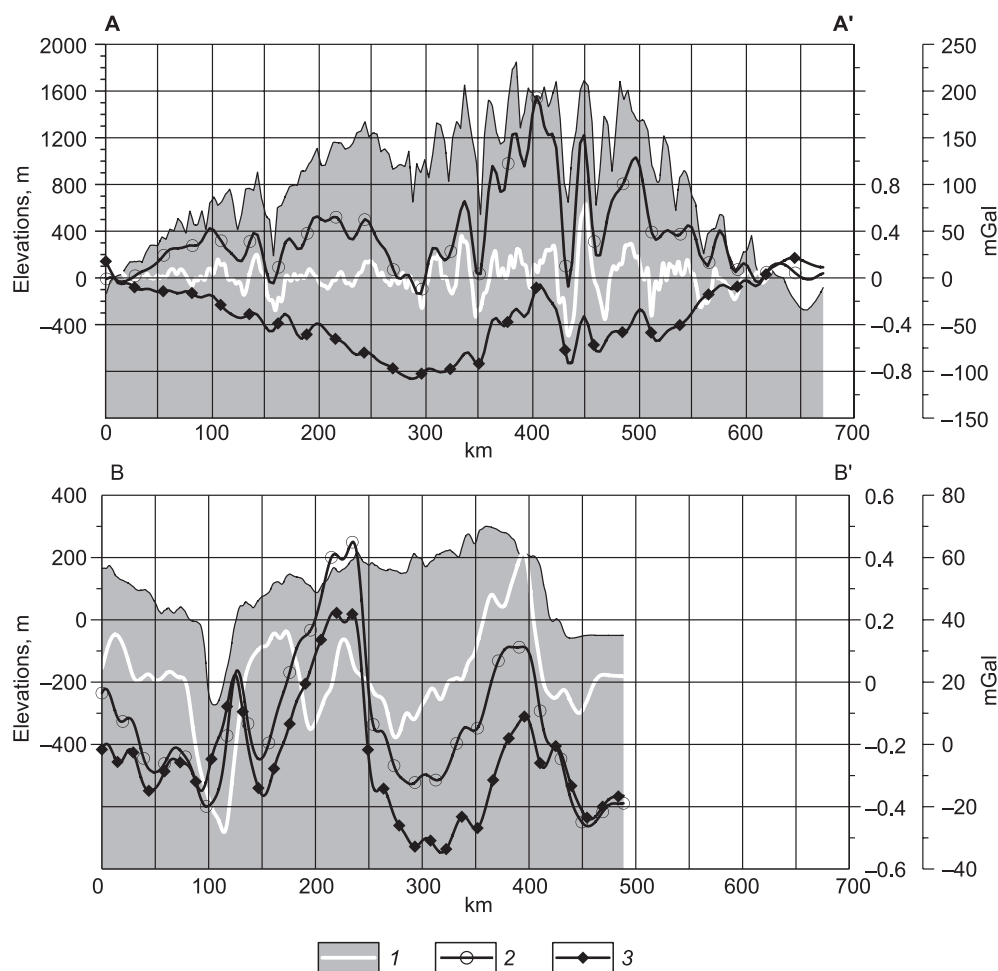


Fig. 10. Top panel: profile A–A' across South Norway (Figs. 6–9); bottom panel: profile B–B' across Kola Peninsula (Figs. 13–15). Thin black contour of gray field: elevations (y axis, left). 1, function of 2D Laplacian of relief elevation function (y axis, right, ± 0.8); 2, 3, free-air and Bouguer anomalies, respectively (scale on the right, in mGal).

Uplifted areas with rugged terrain are located in the north, near the Varangerfjord and the Murmansk Fjord, as well as in the central western part of the area from Lake Inari to the Revda–Kirovsk–Apatity–Kandalaksha Gulf. Elevations reach 1110 m asl southwest of the Nordkin Cape and about 400–600 m at Kovdor, both at the divide along the Russia–Finland and Norway–Finland national frontiers. The elevations reach 1050–1140 m in the Khibiny Mountains near the cities of Kirovsk and Apatity. The rugged faulted surface of the Rybachii Peninsula and the Murmansk Fjord resembles that of South Norway (Fig. 3). The Murmansk Fjord and the Kandalaksha Gulf are areas of moderate seismic activity (Panasenkov, 1969; Nikolaeva, 2001; Asming et al., 2010).

The area farther in the south till 68° N (Fig. 11a) is a combination of highest round uplifts between 36° and 40° E with numerous small blocks. The Kandalaksha–Apatity–Khibiny (Kirovsk) territory is heavily faulted (Fig. 11b). The faults (black lines) mapped according to the geological map (Mitrofanov, 2012) and a similar figure in the study of

Nikolaeva et al. (2018), delineate circular and elongate blocks: the 50×40 km Khibiny and 30×20 km Polarnye Zori blocks; the 40×10 km Apatity block east of the Kola Nuclear Power Station; the 40×20 km Khibiny blocks; and the 25×10 km Kandalaksha Gulf block similar to large blocks in highlands and near the coast (Fig. 6).

The somewhat tentative tectonic framework enlarged in Fig. 11b (red lines) consists of small or medium blocks (10×3 to 2×3 km, or 6×4 km on average), like those in Fig. 6. They correspond to glacial lakes, bays in the Kandalaksha Gulf, and landforms prominent on its sides (Khibiny Mountains, Chunutundra and its northwestern surroundings) but poorer detectable in-between.

The uplifted area near Lake Chunozero and the Kola Nuclear Power Station (Fig. 11b) is dissected by 400–1000 m long, 50 m wide, and 30 m deep fissure-like local zones of extension, possibly pull-apart basins (Evzorov and Nikolaeva, 2003; Nikolaeva et al., 2018), on the background of the general strike-slip style of deformation (Fig. 12). Similar or larger local extension zones (up to 2.0–2.5 km long and

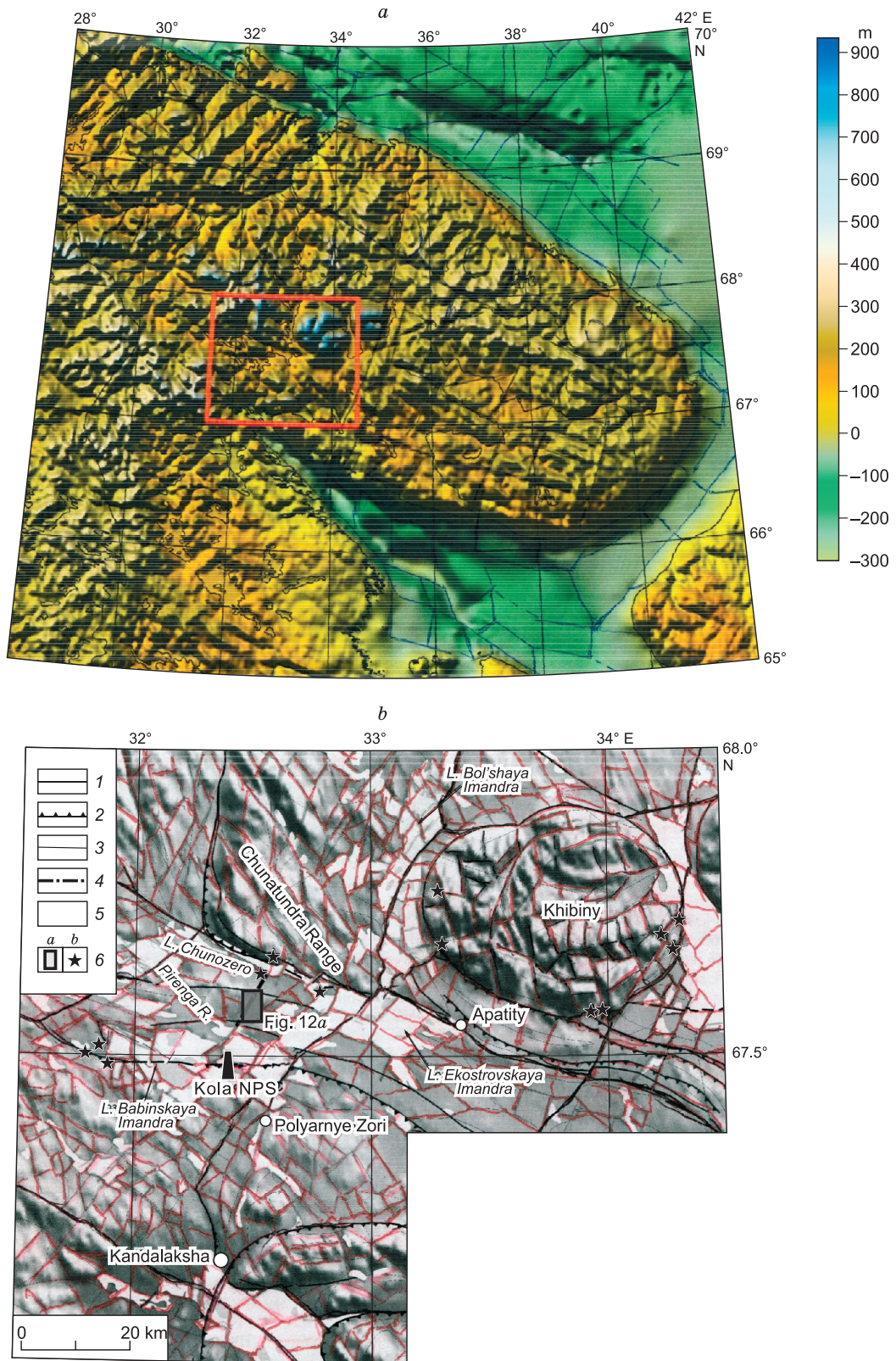


Fig. 11. *a*: shadow relief model of the Kola Peninsula and its surroundings; *b*: enlarged structure of area in red box (Khibiny Mountains and Kandalaksha Gulf). *a*: red box frames zone of Fig. 11*b*; blue thin lines: offshore and adjacent onshore block boundaries; *b*: 1–4, boundaries of main geodynamic zones (1), faults with hatches toward slip plane dip (2), boundaries of subsidiary geodynamic zones (3), and fault segments reactivated in postglacial time (4); 5, water; 6*a*, site enlarged in Fig. 12, 6*b*, fault scarps produced by past earthquakes (Mitrofanov, 2012; Nikolaeva et al., 2018).

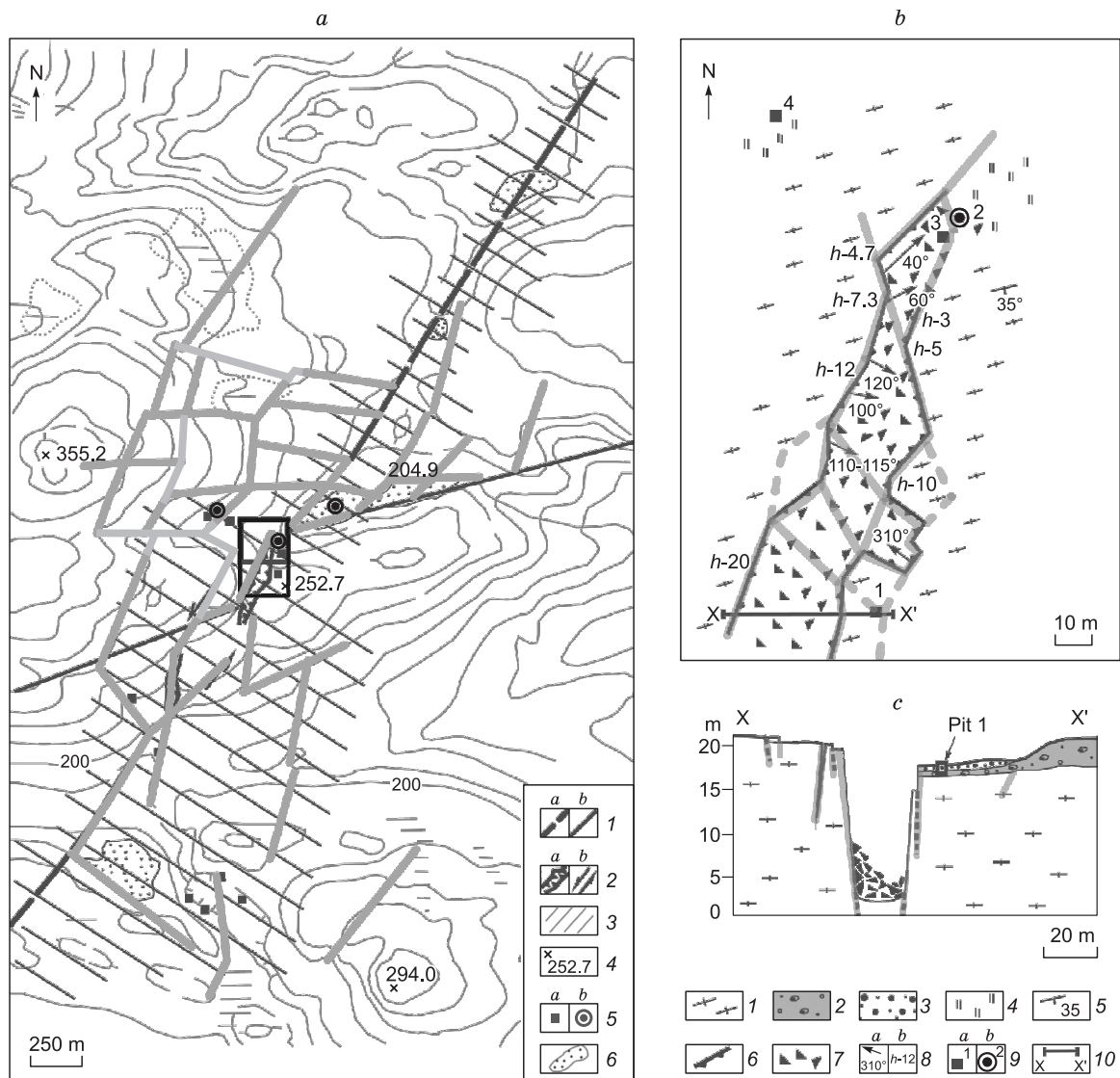


Fig. 12. Seismotectonic map (Nikolaeva et al., 2018) and enlarged structure of red box from Fig. 11b. *a*: 1, main (*a*) and subsidiary (*b*) active faults; 2, canyons (*a*) and strike-slip faults (*b*); 3, deformed zones; 4, elevations (m, asl); 5, sampling sites of soft sediments: trenches (*a*) and boreholes (*b*); 6, lakes; elevation contour lines, at 20 m; box frames area enlarged in panel (*b*); *b*, *c*: 1, gneiss granite; 2, moraine; 3, fluvial-glacial deposits; 4, marsh; 5, bedding angle and dip; 6, fault scarps; 7, rock falls; 8, strike azimuths of long axes of rock falls (*a*), scarp heights, m (*b*); 9, trenches (*a*); boreholes (*b*); 10, line of profile X–X'. Heavy gray lines are block boundaries (similar to red lines in Fig. 11b).

50–100 m deep) were reported from Wisconsin, USA (see below). At least some of the Fennoscandian fjords, which follow the mosaic structure of the uplift and only partly surround its highest part, are such extension structures, especially the large ones reaching 200 km long (Fig. 6). On the other hand, V-shaped glacial valleys in mountains are more straight, wide at the top and narrow at the bottom (vice versa in fjords) and fall off the mosaic structure (Fig. 6). Thus, the zones of extension vary in lateral size from 200 km to 1–2 km and from 2 to 0.1 km in depth depending on the extent and rate of uplift. Note that the patterns associated with extension and uplift are similar: e.g., the mosaic of 0.3–3.0 km blocks in Fig. 12a resembles the pattern with 5–30 km blocks in Fig. 11b and c.

The map of transformed elevations (Fig. 13) was compiled using averaging suitable for its further correlation with gravity anomalies (Fig. 14). Free-air gravity anomalies in the Kola Peninsula range from –50 to +56 mGal with a twice smaller contrast than in Norway (Fig. 8): 106 mGal against 200 mGal. They have more curved and less distinct contours than their Norwegian counterparts (Fig. 8), but there are prominent round highs related to the Khibiny and Lovozero alkaline intrusions, as well as to the Chunutundra, Monchegorsk, and Fedorovo mafic-ultramafic intrusions.

Large 300–400 km gravity lows have circular shapes in the center of the Kola Peninsula and are rather square near the Barents Sea coast, where they may record young rift-related deposition. Another low in the Kola Peninsula is en-

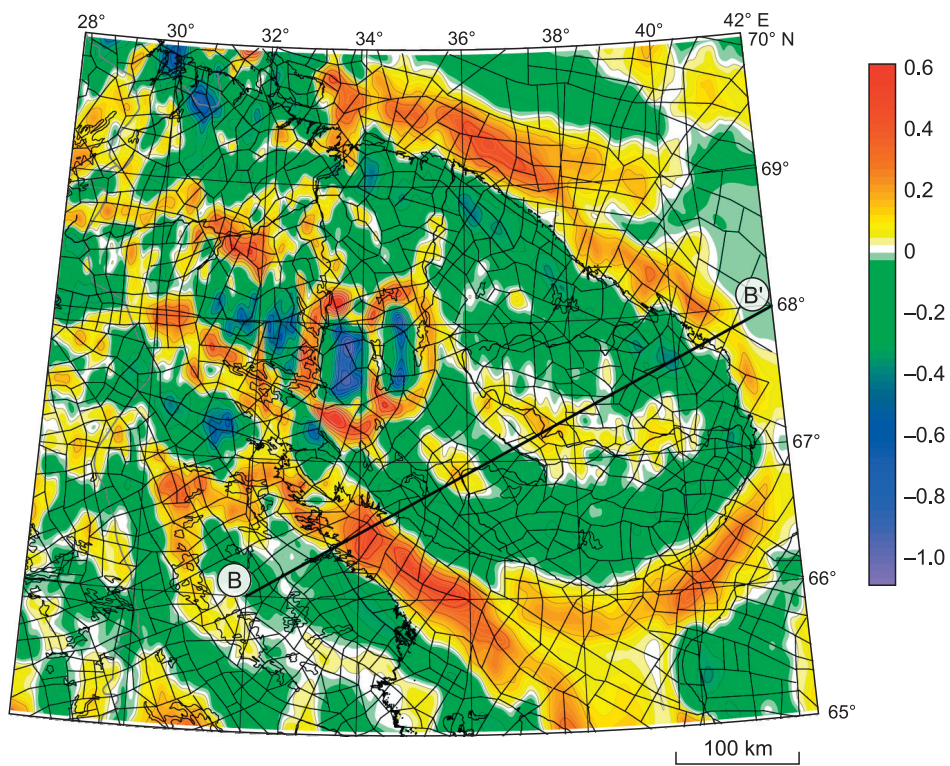


Fig. 13. Transformed surface topography of the Kola Peninsula and its surroundings (normalized 2D Laplacian). Line B–B' is profile shown in Fig. 10.

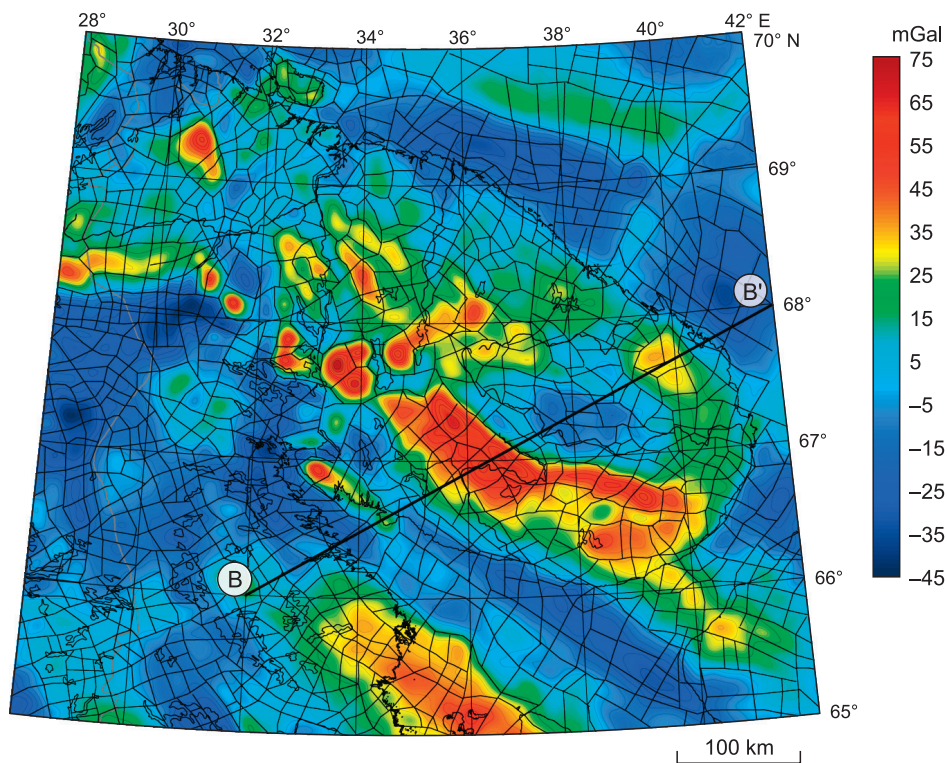


Fig. 14. Free-air and Bouguer gravity anomalies of the Kola Peninsula and its surroundings. Thin lines: polygonal mosaic pattern based on gravity and surface topography maps, with reference to the DTU15 global model (Anderson and Knudsen, 2016).

circled by highs and has a different nature. The pattern of free-air anomalies is consistent with the map of transformed terrain elevations (Fig. 13).

The Bouguer anomalies in the Kola Peninsula (Fig. 15) generally agree with the free-air gravity anomalies (Fig. 14) but are shifted toward positive values and are wider. There are distinct anomalies in the northwestern coast of the peninsula and a narrow low-gravity zone in the northern side of the Kandalaksha Gulf, along the boundary of the Beloe Sea orogenic area, which ends in northwest with an oval feature. Compared with the surface topography, the Bouguer gravity anomalies appear to be largely controlled by crust density variations, with an effect of uplift roots traceable in the peninsula center.

At least seven oval-shaped anomalies, from 500 to 250 km (Figs. 14 and 15), better pronounced in the Bouguer gravity pattern (Fig. 15), are main features of the Kola gravity field. The largest Murmansk anomaly about 500 km in diameter (left top corner) is cut by the Murmansk Fjord (Fig. 5). There is a +40 mGal high in the center, at the intersection of the 30° E longitude and 69° N latitude, surrounded by a yellow-green zone of –5 to –30 mGal and again by a 0 to +40 mGal positive feature.

Another large Bouguer anomaly occupies the southeastern half of the Kola Peninsula, but the center of the peninsula is marked by a prominent low to –50 mGal encircled with a high of +60 mGal. These anomalies coexist with four smaller features: two lows in the Barents and Beloe Seas

and two anomalies farther in the west. The circular anomaly adjacent to the Kandalaksha Gulf and that of the Barents Sea are located half offshore and half onshore and both have elongate highs in the center. Two more small round anomalies, likewise with positive anomalies in the center, are located between the Murmansk and Kandalaksha anomalies and southeast of Kandalaksha.

In the first approximation, the Kola gravity anomalies (Figs. 14 and 15) are similar to the Bouguer and especially free-air gravity anomalies in South Norway (Figs. 8 and Fig. 9), but different for the round highs in the center of continental Bouguer anomalies (Fig. 15). The South Norway anomalies correspond to the Caledonides and may be associated with the respective orogenic crust thickening, whereas the zoned features in the Kola Peninsula may record the Archean Belomorian or partly Saamian orogenies. The simple anomalies, without highs in the center (including three offshore features), may represent Quaternary glaciation, while the complex features are of unclear origin and might be due to plume-related magmatism.

The curves of free-air and Bouguer gravity anomalies are conformal in the coordinates of distance-dependent elevations where they are plotted together with the 2D Laplacian function of relief height function (Fig. 10) along profile B–B' (Figs. 13–15). This conformity is due to a relatively low local topography variation (mostly <100 m local relief) and, correspondingly, small local terrain corrections in the Bouguer data, except for the Kandalaksha Gulf area between 90

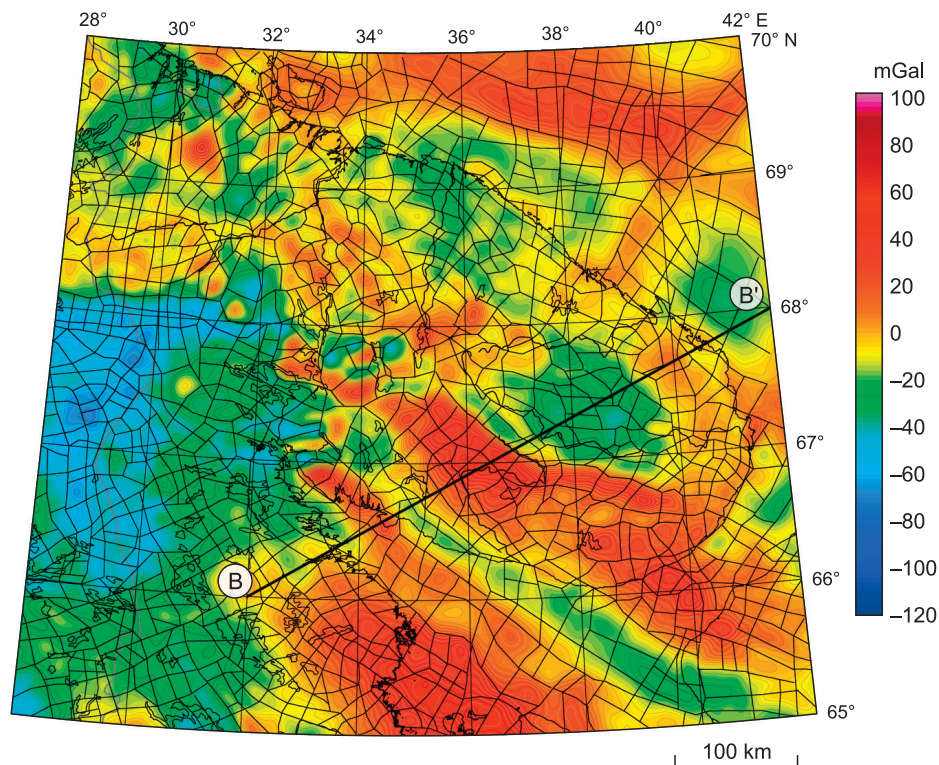


Fig. 15. Bouguer gravity anomalies of the Kola Peninsula and its surroundings based on the EIGEN-6C4 global model (Förste et al., 2014). Thin lines: polygonal mosaic pattern.

and 120 km. However, the behavior of elevations and gravity correlate well only within small ≤ 50 km zones of local elevation changes that match local gravity anomalies. The curve of 2D Laplacian of relief elevation function (white line) agrees well with the behavior of both gravity anomalies, but moderate topographic heights correspond to gravity lows in the area between 125 and 175 km where the rocks of the Kolvits–Umba granulite-gneiss belt may have low density (Glaznev et al., 2015; Korsman et al., 1997). Note also that local Bouguer anomalies have greater magnitudes than the initial free-air anomalies, contrary to their relation in South Norway (profile A–A'). The only reason may be that rocks in small landforms are less dense. The Bouguer gravity curve for the Kola Peninsula has a smooth 20–25 mGal bending (Fig. 10, bottom panel), which records the root compensation effect of topography uplift, like that along the A–A' profile (top panel).

POSTGLACIAL UPLIFT IN THE CANADIAN SHIELD (WISCONSIN, USA)

The Canadian shield is an area of large-scale postglacial uplift (Fig. 16) which correlates with ice thickness. Glaciation in the Canadian shield began about 6 Ma (Eyles, 1993) and postdated the Cordillera ice sheet on the Pacific coast. Melting of the latter produced totally 22,000 km³ of sediments on the shore and 1218,000 km³ or 55 times more in the offshore areas (Eyles, 1993; Lisitsyn, 2001), out of which about 300,000 km³ on the shelf (12 times more than onshore) and more than 800,000 km³ on the continental slope. These values are essential for assessment of the glaciation extent.

The Canadian ice sheet (Fig. 16a, b), called also the Lawrence ice sheet after the Gulf of St. Lawrence, produced in total 105,000 km³ of glacial deposits, mainly moraines (Fig. 16a). About 1023 km³ of sediments deposited on the sea bottom, mainly on the shelf and partly on the continental slope, half-circle the glacier and the zone of moraines. The amount of offshore deposition is eleven times the onshore volume and is commensurate with that on the shelf near the Cordilleran ice sheet (Eyles, 1993; Lisitsyn, 2001). The flux of glacial sedimentary material consisted of two parts (Lisitsyn, 2001): one associated with onshore ice melting and ensuing sediment transport to the land and shelf areas, and the other due to offshore ice growth leading to the formation of brines which carry large amounts of suspended matter (nepheloid layer) and control near-bottom masses and currents, including the cold near-bottom equivalent of Gulf Stream. The nepheloid sedimentary flux has been better studied on the Pacific coast, while the amount of pelagic sediments in the Atlantic Ocean may be underestimated.

The ice thickness on the Canadian shield and related uplift (Fig. 16b) had several peaks: one main peak >3 km within the Hydson Gulf where the total uplift is above 900 feet (300 m), and five subsidiary peaks. The five peaks include

two in the area of Great Lakes, one northwest of Newfoundland with ~500 ft (170 m) uplift, and two within and south of Baffin Island (>700 ft or 220 m uplift).

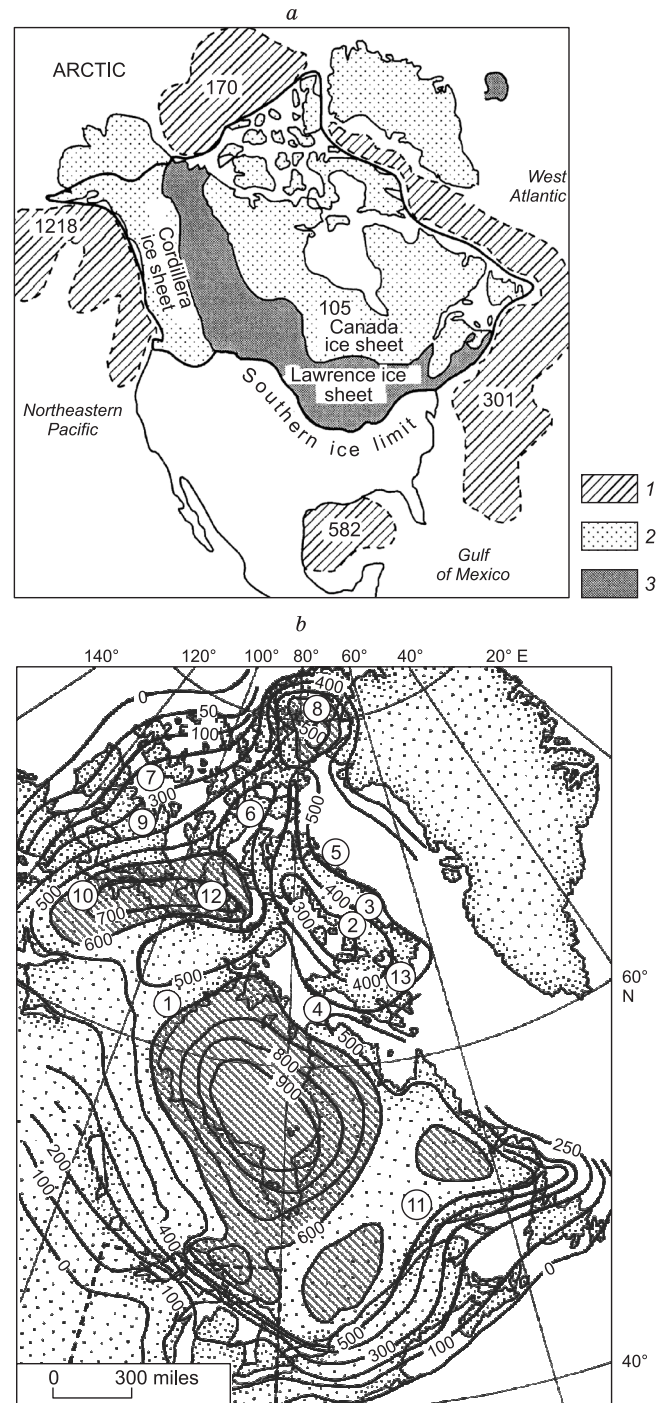


Fig. 16. a: Ice sheets in North America, amount of glacial deposits on the continent and on the sea bottom, in thousands of km³ (Eyles, 1993; Lisitsyn, 2001); b: amount of postglacial uplift (in feet) in North America (Innes and Argun-Weston, 1966), modified after (Artyushkov, 1979) and our data. a: 1, glacial gravity flow deposits in oceans; 2, onshore glaciation zones; 3, main onshore moraine deposits; b: uplift rate, in m. Dash line box in the panel bottom is area enlarged in Fig. 18.

It is impossible to assess and characterize all details of postglacial uplift over the whole enormous territory about 3000 miles long within the scope of this paper, and we confine ourselves to the area of Great Lakes and their southern surroundings (hatched partly in Fig. 16b) which encompasses the states of Wisconsin, Michigan, and Illinois. The glaciation was the most prominent in Wisconsin and is called correspondingly. Yet, even this limited area experienced several episodes and numerous phases of glaciation (Larson and Kincare, 2009; Curry et al., 2011; Larson, 2011; Syverson and Colgan, 2011).

The limits of glaciation are shown in the map of bedrock geology (Fig. 17a), modified after (Mickelson and McCartney, 1979; Marshak et al., 2016), which is currently buried under Quaternary glacial deposits. Blue dash line contours the southwestern boundary of the Wisconsin glaciation (Dyke, 2004) and the solid line delineates the limits of the earlier Illinois glaciation (Larson, 2011). The maximum postglacial uplift coincides with the Precambrian basement uplift in the northern Wisconsin where its faulted polygonal pattern with block sizes about 10–15 km by 3–10 km is clearly pronounced. The uplift is surrounded by a zone of subsidence filled with thick Cambrian–Ordovician and Quaternary sediments, without division into blocks. The polygonal pattern reappears near the ice boundary, within the zone of exposed Late Cambrian metamorphic rocks of the North Illinois uplift, as well as in Cambrian–Ordovician sediments around both uplifts. The section A–A' across this zone (Fig. 17b) shows the faulted basement top and heavily deformed Late Precambrian quartzite.

Our free-air gravity map based on the DTU15 global model (Andersen and Knudsen, 2016) covers a larger territory including most of the Great Lakes area in North America (Fig. 18). The white line contours the geological map of Illinois and Wisconsin (Fig. 17), the black heavy line is the boundary of the Illinois glaciation (Larson, 2011), the dash line shows the limits of the Wisconsin glaciation (Dyke, 2004), and thinner black lines are two profiles chosen for a more detailed discussion of gravity features. The polygonal mosaic pattern is well evident over the craton between the Appalachian and Duluth orogens on the southeast and the northwest, respectively, which themselves have a linear structure crosscutting the fault blocks.

The Precambrian basement uplift in the northern Wisconsin state and the adjacent part of Michigan is marked by four gravity highs up to +75 mGal and three similar highs in the state of Michigan between lakes Michigan and Huron correspond to local Precambrian uplifts. They make up a circle with a double low (to –75 mGal) in the center. In general, this zoned gravity feature with a 150 mGal contrast (–75 to +75 mGal) matches the local glaciation center shown in Fig. 16, and is in some respect similar to the oval features in South Norway (Figs. 6 and 9) and in the Kola Peninsula (Fig. 15). The large gravity lows (Fig. 18) are similar to upper mantle anomalies in North America (between 48° and 35° N) reported by Mooney and Kaban (2010), but our map is more detailed.

The patterns of elevations (Fig. 18) and gravity anomalies (Fig. 19) along profiles 1 and 2 (profile 2 coincides with A–A' in the geological map of Fig. 17b; Bouguer gravity maps are not shown because they are conformal to the free-air patterns, which is evident in Fig. 19) are related in an intricate way. Local free-air and Bouguer gravity anomalies in profile 1 have positive correlation with local elevation changes. Large topographic features (about 100 km along the profile) show negative correlation with gravity anomalies in the beginning of the profile and positive correlation in its end. The large gravity anomalies along profile 2 are mostly associated with density heterogeneity in the crust (compare with Fig. 17b), while local features correlate with local landforms, either directly or inversely (in some cases, depressions correspond to gravity highs and vice versa). In the same way as for Fennoscandia, conformal variations of local Bouguer anomalies may indicate similarity in their origin. Glacial motions may have caused nonuniform uplift and subsidence of adjacent blocks which brought to the same hypsometric level rocks of different densities, or these blocks themselves became subsided or uplifted at different rates.

Although the gravity record of glaciation in the Canadian shield is fragmentary (Fig. 18), it generally confirms the analogy with the Fennoscandian uplift as to the presence of local glaciation centers and postglacial polygonal mosaic patterns, as well as oval Bouguer anomalies at the crust–mantle boundary above these centers.

DISCUSSION AND CONCLUSIONS

Recent overviews have given much attention to the rate and amount of current postglacial uplift evaluated using GPS (Fig. 2), as well as to related seismicity (Olsen, 1988; Fjeldskaar et al., 2000; Milne et al., 2001; Johansson et al., 2002; Ojala et al., 2004; Lidberg et al., 2010; Simon et al., 2018). Yet, detailed maps of gravity anomalies based on spaceborne data and advanced global models remain insufficiently used, possibly because no global models of the gravity field that would approach the 1:1000000 resolution of the Bouguer gravity maps (suitable for tectonic division) were available before the publication of the WGM 2008 model with averaging over a 5" grid.

The response of the crust to ice loading and unloading (Fig. 20) was associated with stress change from vertical compression (subsidence) during glaciation to postglacial decompression and extension (Johnston et al., 1998; Stewart et al., 2000; Ojala et al., 2004; Simon et al., 2018). Importantly, compression rejuvenated preexisting fractures while extension initiated uplift in a system of blocks, such as Norwegian fjords in the center and local extension fractures on the periphery (Figs. 3, 10a, b, 15b, c), which is confirmed by a contrasting polygonal pattern in gravity maps. The glacial–postglacial subsidence and uplift can be expected to reactivate a part of older tectonic structures.

Ice loading modified preglaciation structures resulting from thickening at the crustal base and others (Figs. 5, 9,

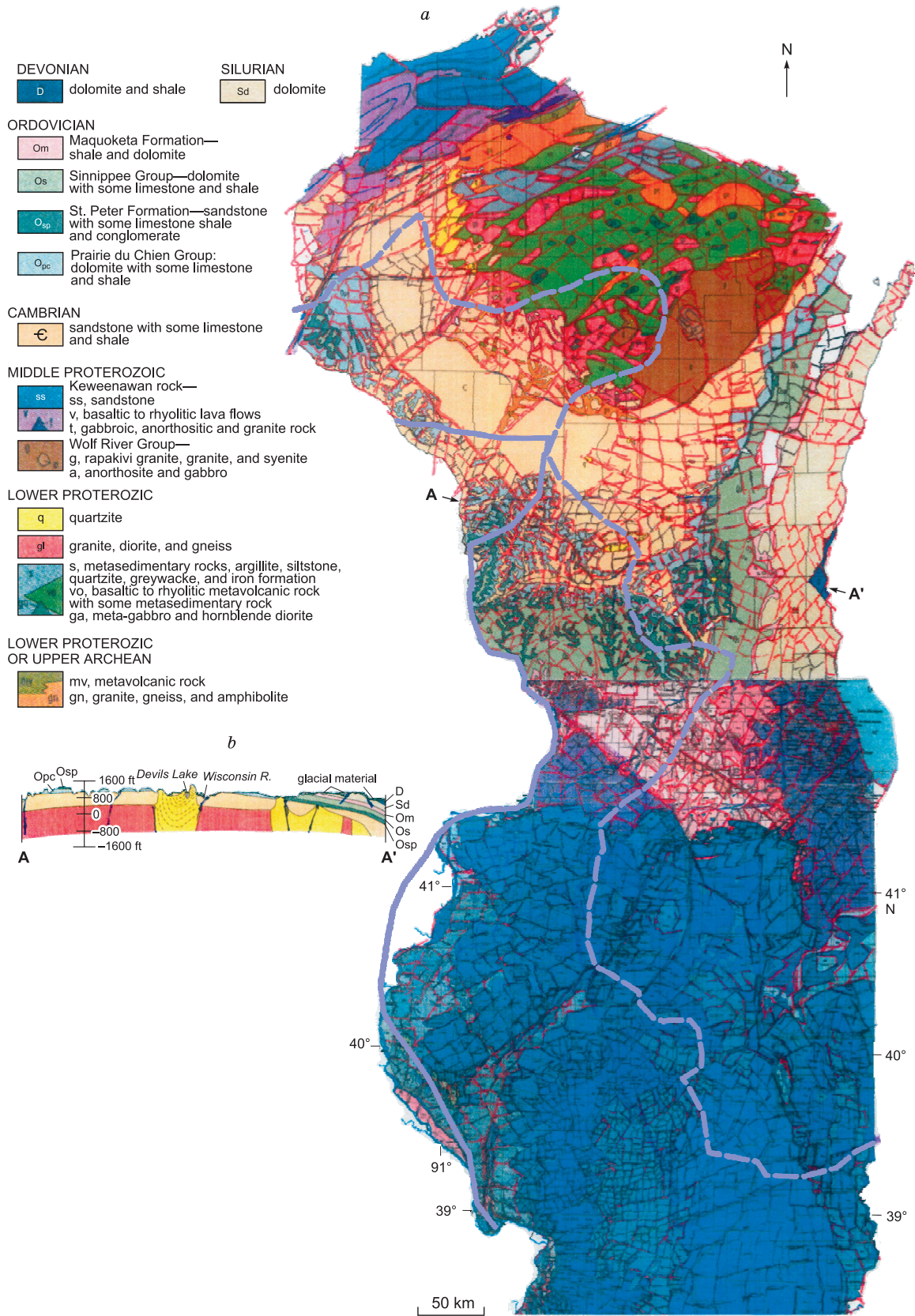


Fig. 17. *a*: geological map of Wisconsin and Illinois, USA; *b*: cross section along line A–A' (Marshak et al., 2016). Blue heavy dash line and heavy solid line: limits of the Wisconsin (Dyke, 2004) and Illinois (Larson, 2011) glaciation, respectively.

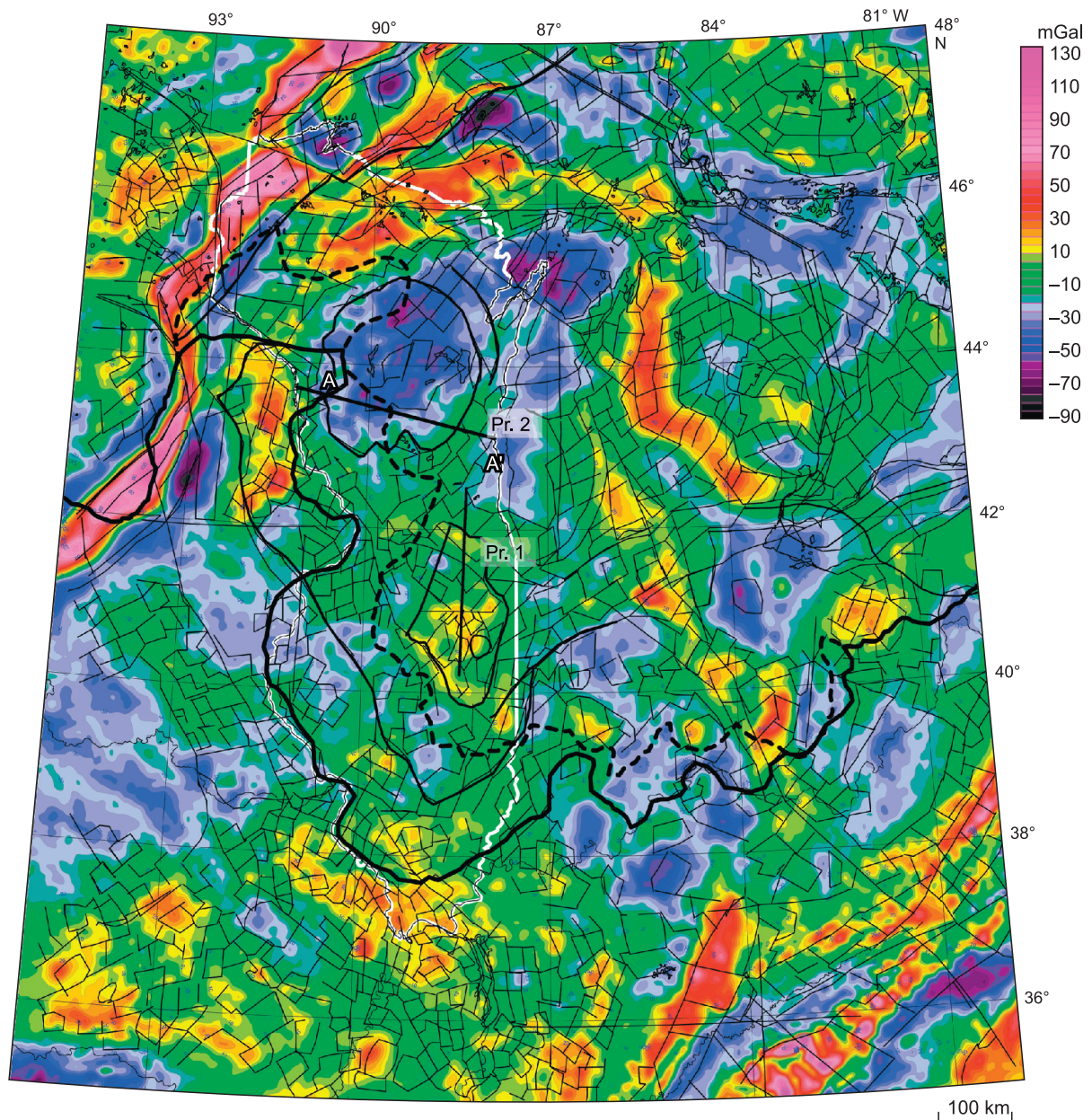


Fig. 18. Free-air gravity anomalies of the Great Lakes area, North America. Compiled with reference to the DTU15 global model (Anderson and Knudsen, 2016). Thin lines: polygonal mosaic pattern within the zone of Wisconsin glaciation and between tectonic belts (northeastern and south-southwestern corners); white contour: geological map of Fig. 17. Black dash and solid lines: limits of Wisconsin (Dyke, 2004) and Illinois (Larson, 2011) glaciations, respectively.

18), which produced deep structures similar to the shallow ones. The similarity between structures in the upper, middle, and lower crust is of course incomplete (Figs. 5, 9, 15, 18). As we have found out, the upper crust and lower crust features (oval structures and blocks) of the postglacial deformation pattern appear, respectively, in the free-air (Figs. 4, 8, 14, 18) and Bouguer (Figs. 5, 9, 15) gravity anomalies in the digital maps compiled with reference to global models based on spaceborne data. More complete interpretation requires joint use of geological data and modeling.

According to the model of a multistage glaciation history (Fig. 2), the formation of ice sheets in Eurasia peaked at

120–150 kyr BP, 80–90, about 60 and 20 kyr BP. They were the thickest and largest at 140 kyr BP, reduced to 15% of the former area in Europe (part of Fennoscandia) at 80–90 kyr BP, and recovered to 70–80% at ca. 20 kyr BP; the Kara ice sheet in Asia became only ~30% smaller at 80–90 kyr BP and reduced to 35–40% of its former area at 20 kyr BP (Fig. 1). As a result, multiple glacial centers with different ice thickness appeared and disappeared, migrated over the territory (Grosswald, 1999; Ojala et al., 2004; Svendsen et al., 2004; Simon et al., 2018; etc.).

Modeling of the Fennoscandian ice sheet history (Siegert et al., 2001; Svendsen et al., 2004) indicates that ice was the

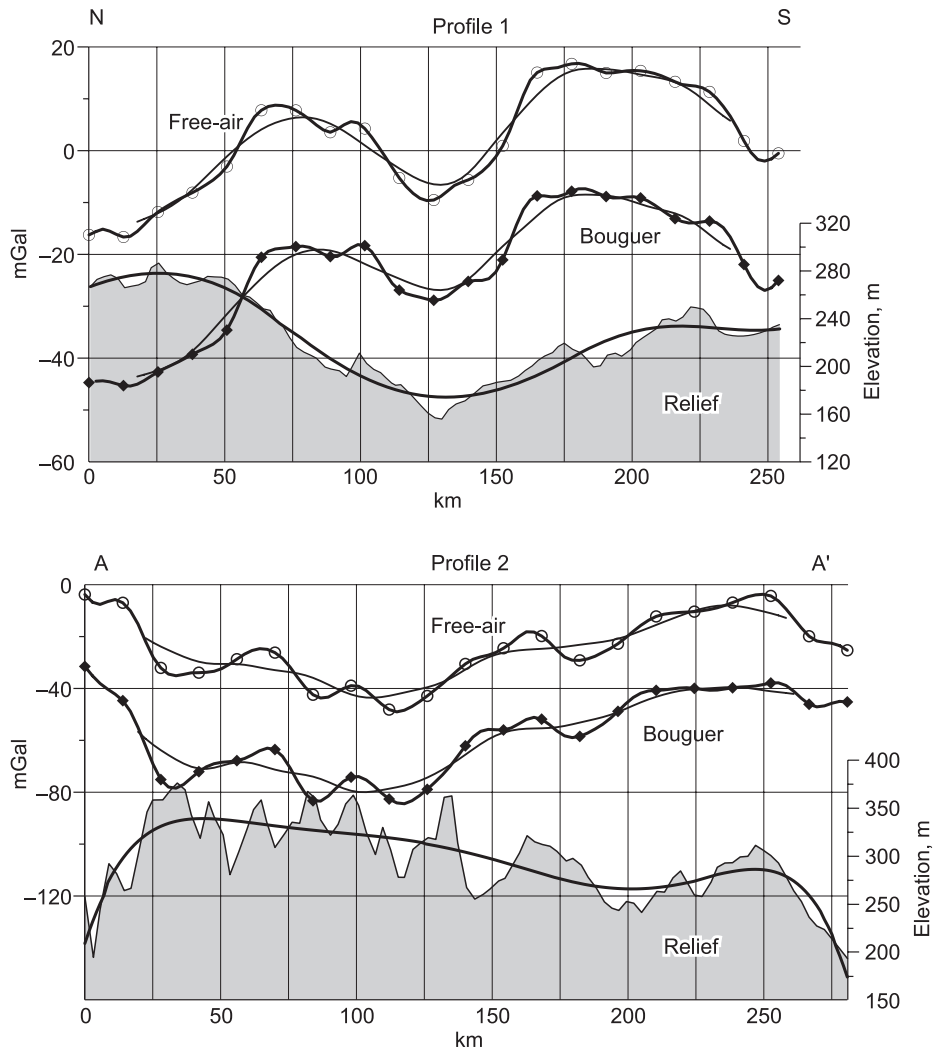


Fig. 19. Elevations and free-air and Bouguer gravity anomalies along profiles 1 and 2. Thin black lines: smoothed gravity profiles; heavy black line: approximating spline of elevations. For location of profiles see Fig. 18.

thickest (3100 m) in South Norway at 140 kyr BP; then the maximum moved to Finland at 90 kyr BP and to the boundary between South Sweden and Norway at 60 kyr BP (1750 m the thickest); 20–15 kyr BP, the thickest ice of 2800 m was within the Gulf of Bothnia, i.e., near points 1, 3, 4 and 6 in Fig. 2. It reached the maximum thickness of >2800 m as centers 1, 3 and 6 coalesced (Siegert et al., 1999). The center with 2.6 km thick ice was in South Sweden when the last ice sheet began melting 14 kyr BP ago; then it moved to the Baltic Sea at 12 kyr BP, and then to North Finland at 11 kyr BP, where its thickness reduced to 1.5 km; most of the ice had melted about 9 kyr BP (Forman et al., 2004).

Understanding which event of the ice sheet history caused the greatest influence on the gravity pattern requires additional data. Most likely, it was a joint effect of several events, but one or another was predominant in each area. For instance, the 80–90 and 120–140 kyr events left the most prominent imprint in South Norway while Finland stores mainly the record of the latest 15–20 kyr BP glaciation.

The problem can be solved by studying local tectonic and seismicity effects (Fig. 21), including stress distribution: main horizontal stress components (large arrows) and orientations of compression (P, black dots) and tension (T, white dots) axes (Simon et al., 2018). The polygons either traverse earthquakes (or their clusters) or follow “average” structural lines. In the pattern of principal stress tensor axes (Chen, 1991; Ojala et al., 2004; Simon et al., 2018), zones of nearly zero stress (ovals in Fig. 21b) match those with rare or absent structural lines (blue polygon contours in Fig. 21a). The fields of predominant tensile stress (thin lines, blue shade) are more abundant in northern Finland or are equal to the fields of compression (heavy lines, green shade). The pattern in Fig. 21 is consistent with the structural pattern of Finland in Fig. 4. Since earthquakes characterize the current stress patterns, the tectonic features (Figs. 4, 5) confirm that they record present or recent deformation associated with postglacial uplift. Figures 4, 5 and 21 do not match perfectly because the structures in the gravity maps are multistage.

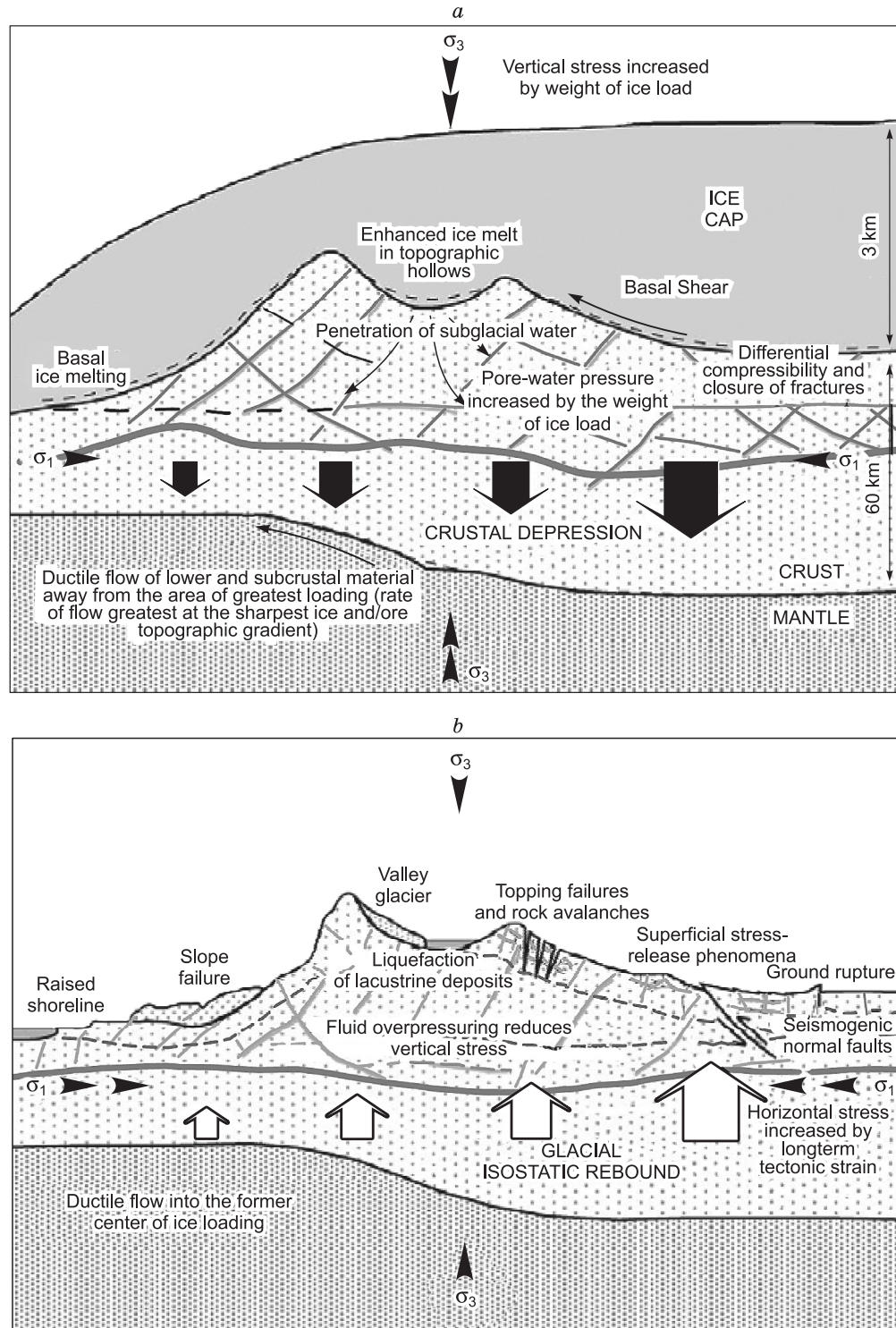


Fig. 20. Impact of glacial loading (a) and unloading (b) on the crust: sketch models, complemented and updated after (Stewart et al., 2000; Ojala et al., 2004; Simon et al., 2018). Exaggerated vertical scale difference between the crustal thickness (~60 km) and ice-sheet thickness (~3 km). Note stabilization of structures during ice rebound, increase of vertical stress during glaciation when $P_{\text{tot}} = P_{\text{lit}} + P_{\text{ice}}$; decrease of vertical stress ($P_{\text{tot}} = P_{\text{lit}} - P_{\text{ice}}$) and increase of differential stress (σ_1 and σ_2) after glaciation.

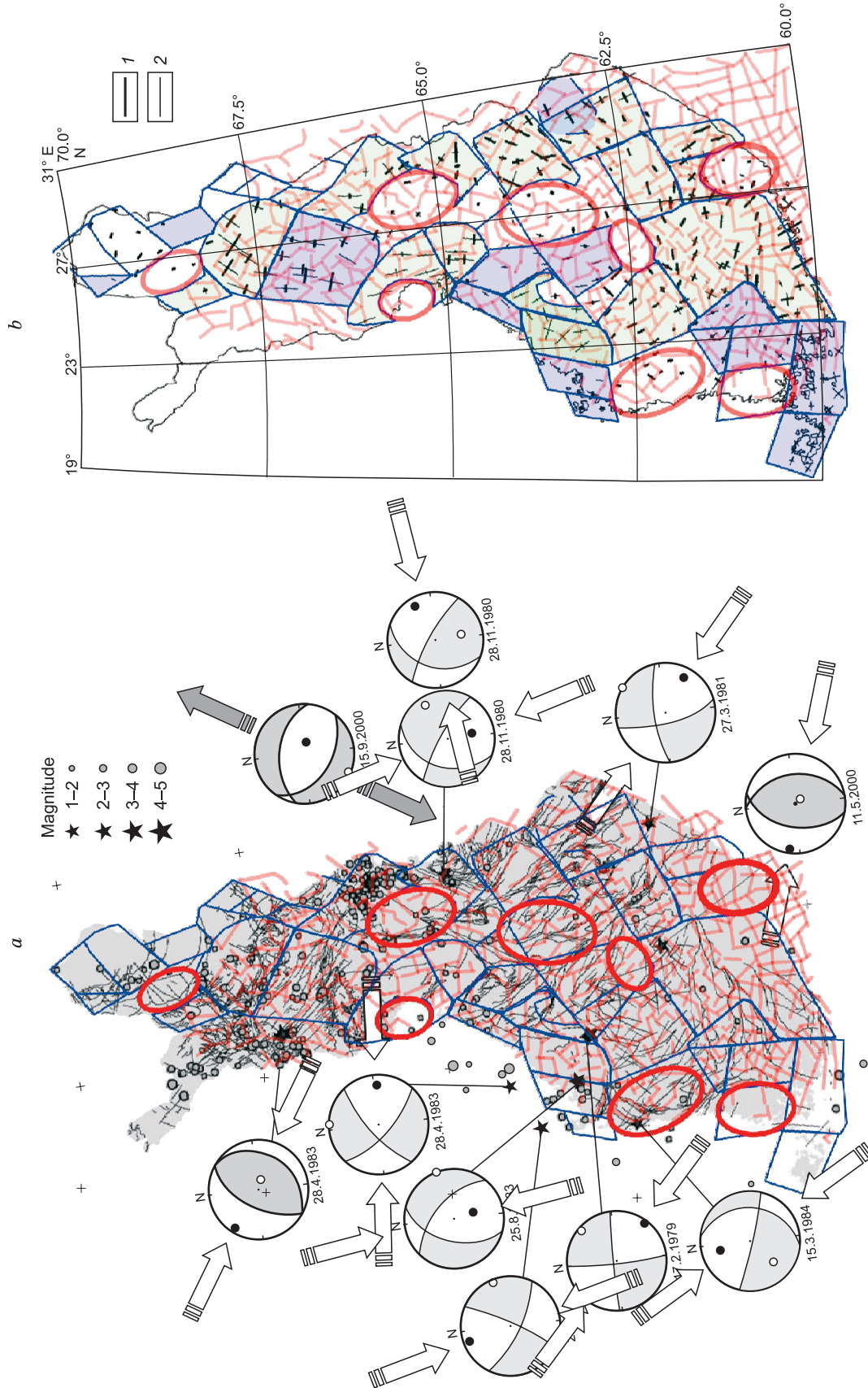


Fig. 21. *a*: seismotectonic map of Finland (Korsman et al., 1997), earthquakes and their mechanisms (fault plane solutions); *b*: stress directions and magnitudes (Chen, 1991; Ojala et al., 2004; Simon et al., 2018). Earthquakes are marked by gray circles and stars, with their sizes proportional to magnitudes. Pale red lines delineate mosaic pattern from Fig. 4. Principal strain: *I*, compression, at $-0.4 \mu\text{m}/\text{yr}$; 2, extension $+0.4 \mu\text{m}/\text{yr}$. See text for explanation.

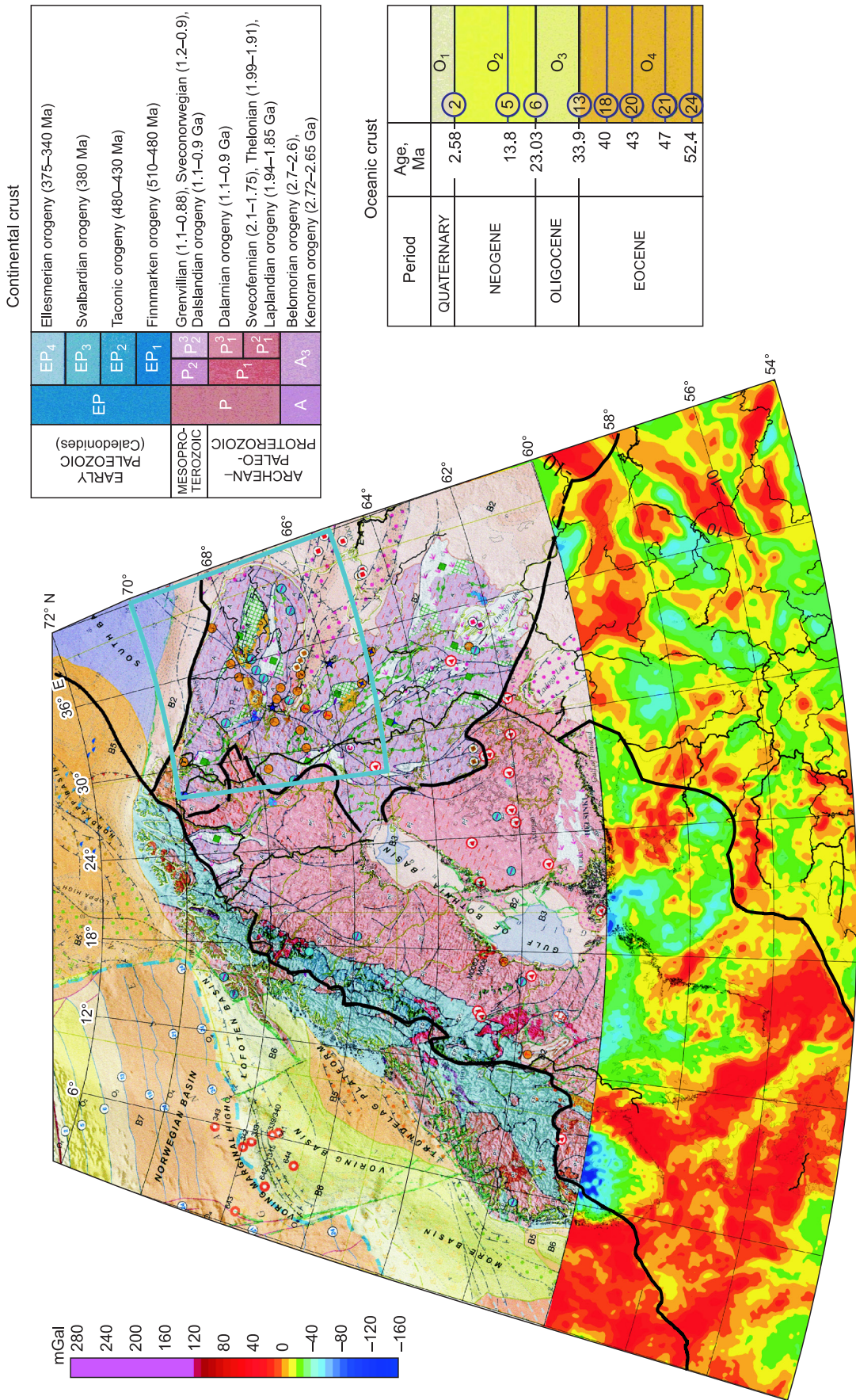


Fig. 22. Tectonic map of the Arctic region and a fragment of Bouguer gravity map (south of 60° N). Heavy black line: limits of tectonic areas; blue line: Kola Peninsula shown in gravity maps of Fig. 14 and 15.

The example models of Figs. 20 and 21 are rather an introduction into the problem than a final solution. Like the reported gravity maps, they provide the first but essential contribution into understanding of postglacial uplift and the related tectonic and deposition framework. However, gravity data cannot provide time constraints, which are especially important when several postglacial uplift events are considered. No solution is however possible in this respect without data on geology and geomorphology recorded in sediments of different ages. The effect of these processes may be related with variable lithospheric viscosity.

We have gained some experience in the use of gravity maps for analyzing zones of ongoing compression from Lake Baikal to the Himalayas (Dobretsov et al., 2016, 2017; Dobretsov and Vasilevskiy, 2018). The compressional structures of the Baikal, Tien Shan, Tarim, and Pamir regions that formed as a remote response to the India–Asia collision appear to be surprisingly similar to the extension structures associated with postglacial uplift in Fennoscandia. This is only geometrical similarity though, while the driving forces and intensity of deformation differ markedly. Specifically, the Baikal-type compression structures have distinct boundaries in gravity maps (almost without transition zones), and are related to both uplift and deep subsidence. The similarity of extension and compression structures in these geographically dispersed areas may be due to the presence of similar pre-existing deformation patterns (Fig. 3) like that of the East European craton.

The Scandinavian fragment of the International Tectonic Map of the Arctic region (Petrov and Pubellier, 2018) juxtaposed with our Bouguer gravity map (Fig. 5) in the south (Fig. 22) show a good match, with oval and angular blocks of different sizes. Structural similarity is likewise evident within the Kola Peninsula (blue box), same as in the gravity maps of Figs. 14 and 15. However, this issue is beyond the present consideration and will be a subject of further research. It will be interesting to discuss geotectonics in the context of the deformation framework.

The paper has profited much from constructive criticism by V.D. Suvorov and I.D. Zolnikov, the reviewers, which we greatly appreciate.

The study made part of Integration Project 51 run by the Siberian Branch of the Russian Academy of Sciences and was carried out on government assignment No. 0331-2019-0010.

REFERENCES

- Andersen, O.B., Knudsen, P., 2016. Deriving the DTU15 Global high resolution marine gravity field from satellite altimetry, in: Abstract from ESA Living Planet Symposium. Prague, p. 1558.
- Artemieva, I.M., Thybo, H., 2013. EUNASEIS: A seismic model for Moho and crustal structure in Europe, Greenland, and the North Atlantic region. *Tectonophysics* 609, 97–153.
- Artyushkov, E.V., 1967. Setting up crustal isostasy. *Izv. AN SSSR, Fizika Zemli*, No. 1, 3–16.
- Artyushkov, E.V., 1971. Rheological properties of the crust and upper mantle according to data on isostatic movements. *J. Geoph. Res.* 76 (5), 1376–1390.
- Artyushkov, E.V., 1979. *Geodynamics* [in Russian]. Nauka, Moscow.
- Artyushkov, E.V., Korikovskiy, S.P., Massonne, H.-J., Chekhovich, P.A., 2018. Recent crustal uplift of Precambrian cratons: Key patterns and possible mechanisms. *Russian Geology and Geophysics (Geologiya i Geofizika)* 59 (11), 1389–1409 (1737–1764).
- Asming, V.E., Kremenetskaya, E.O., Vinogradov, Yu.A., Evtyugina, Z.A., 2010. Criteria for identification of blasts and earthquakes: application to for seismic risk assessment. *Vestnik MGTU* 13 (4/2), 998–1007.
- Chen, R., 1991. On the Horizontal Crustal Deformations in Finland. Reports of the Finish Geodetic Institute, 91:1.
- Curry, B.B., Grimley, D.A., McKay III, E.D., 2011. Quaternary glaciations in Illinois, in: Ehlers, J., Gibbard, P.L., Hughes, P.D. (Eds.), *Quaternary Glaciations—Extent and Chronology: A Closer Look. Developments in Quaternary Science*, Vol. 15. Elsevier, Amsterdam, pp. 467–487.
- Dobretsov, N.L., Vasilevskiy, A.N., 2018. Gravity field, surface topography, and volcanic complexes of Kamchatka and its junction with the Aleutian arc. *Russian Geology and Geophysics (Geologiya i Geofizika)* 59 (7), 780–802 (972–999).
- Dobretsov, N.L., Buslov, M.M., Vasilevskiy, A.N., Vetrov, E.V., Nevedrova, N.N., 2016. Cenozoic history of topography in southeastern Gorny Altai: thermochronology and resistivity and gravity records. *Russian Geology and Geophysics (Geologiya i Geofizika)* 57 (11), 1525–1534 (1937–1948).
- Dobretsov, N.L., Buslov, M.M., Rubanova, E.S., Vasilevskiy, A.N., Kulikova, A.V., Bataleva, E.A., 2017. Middle–Late Paleozoic geodynamic complexes and structure of Gorny Altai and their record in gravity data. *Russian Geology and Geophysics (Geologiya i Geofizika)* 58 (11), 1277–1288 (1617–1632).
- Dyke, A.S., 2004. An outline of North American deglaciation with emphasis on central and northern Canada, in: Ehlers, J., Gibbard, P.L. (Eds.), *Quaternary Glaciations—Extent and Chronology: Part II: North America. Developments in Quaternary Sciences*. Elsevier, Amsterdam, 373–424.
- Ehlers, J., Gibbard, P.L., 2004. *Quaternary Glaciations—Extent and Chronology, Part I: Europe. Development in Quaternary Science*, Vol. 2. Elsevier, Amsterdam.
- Evzorov, V.Ya., Nikolaeva, S.B., 2003. Quaternary ice sheets in the Kola Peninsula area: seismotectonic implications. *Geomorfologiya*, No. 2, 61–64.
- Eyles, N., 1993. Earth's glacial record and its tectonic setting. *Earth-Sci. Rev.* 35 (1–2), 1–248.
- Fjeldskaar, W., Lindholm, C., Dehls, J.F., Fjeldskaar, I., 2000. Postglacial uplift, neotectonics and seismicity in Fennoscandia. *Quat. Sci. Rev.* 19 (14–15), 1413–1422.
- Forman, S.L., Lubinski, D.J., Ingólfsson, Ó., Zeeberg, J.J., Snyder, J.A., Siegert, M.J., Matishov, G.G., 2004. A review of postglacial emergence on Svalbard, Franz Josef Land and Novaya Zemlya, northern Eurasia. *Quat. Sci. Rev.* 23 (11–13), 1391–1434.
- Förste, Ch., Bruinsma, S.L., Abrikosov, O., Lemoine, J.-M., Marty, J.-C., Flechtner, F., Balmino, G., Barthelmes, F., Biancale, R., 2014. EIGEN-6C4. The latest combined global gravity field model including GOCE data up to degree and order 2190 of GFZ Potsdam and GRGS Toulouse. GFZ Data Services. <http://doi.org/10.5880/icgem.2015.1>.
- Glaznev, V.N., Mints, M.V., Muravina, O.A., Raevsky, A.B., Osipenko, L.G., 2015. Complex geological-geophysical 3D model of the crust in the southeastern Fennoscandian shield: nature of density layering of the crust and the crust-mantle boundary. *Geodyn. Tectonophis.* 6 (2), 133–170. <https://doi.org/10.5800/GT-2015-6-2-0176>.
- Gradmann, S., Ebbing, J., 2015. Large-scale gravity anomaly in northern Norway: tectonic implications of shallow or deep source depth and a possible conjugate in northeast Greenland. *Geophys. J. Int.* 203 (3), 2070–2088.
- Grossvald, M.G., 1999. *Eurasian Hydrospheric Catastrophies and Arctic Glaciation* [in Russian]. Nauchnyi Mir, Moscow.
- Johnston, P., Wu, P., Lambeck, K., 1998. Dependence of horizontal stress magnitude on load dimension in glacial rebound models. *Geophys. J. Int.* 132, 41–60.

- Johansson, J.M., Davis, J.L., Scherneck, H.G., Milne, G.A., Vermeer, M., Mitrovica, J.X., Bennett, R.A., Jonsson, B., Elgered, G., Elosegui, P., Koivula, H., Poutanen, M., Ronnang, B.O., Shapiro, I.I., 2002. Continuous GPS measurement of postglacial adjustment in Fennoscandia. Part I. Geodetic results. *J. Geophys. Res. Solid Earth* 107 (B8), 2157. DOI: 10.1029/2001JB000400.
- ICGEM, International Centre for Global Earth Models. <http://icgem.gfz-potsdam.de/home>.
- Innes, M.J.S., Argun-Weston, A., 1966. Crustal uplift of the Canadian shield and its relation to the gravity field. *Annu. Acad. Sci. Fennica* 92 (A III), 169–176.
- Korsman, K., Koistinen, T., Kohonen, J., Wennerström, M., Ekdahl, E., Honkamo, M., Idman, H., Pekkala, Y. (Eds.), 1997. *Bedrock Map of Finland 1:1 000 000*. Espoo: Geologian Tutkimuskeskus.
- Kotlyakov, V.M., Lorius, K., 2000. Four climate cycles: evidence from Vostok ice cores. *Izv. RAN, Ser. Geogr.*, No. 1, 7–19.
- Kotlyakov, V.M., Arkipov, S.M., Henderson, K.A., Nagornov, O.V., 2004. Deep drilling of glaciers in Eurasian Arctic as a source of paleoclimatic records. *Quat. Sci. Rev.* 23 (11–13), 1371–1390.
- Kukkamäki, T.K., 1975. Report on the work of the Fennoscandian Sub-commission, in: *Problems of Recent Crustal Movement*. Valgus, Tallin, pp. 25–29.
- Landvik, J.Y., Bondevik, S., Elverhøi, A., Fjeldskaar, W., Mangerud, J., Salvigsen, O., Siegert, M.J., Svendsen, J.I., Vorren, T.O., 1998. The last glacial maximum of Svalbard and the Barents Sea area: Ice sheet extent and configuration. *Quat. Sci. Rev.* 17 (1–3), 43–75.
- Larson, G.J., Kincare, K., 2009. Late Quaternary history of the eastern midcontinent region, USA, in: Schaeztl, R., Darden, J., Brandt, D. (Eds.), *Michigan Geography and Geology*. Custom Publishing, New York, pp. 69–90.
- Larson, G.J., 2011. Ice-margin fluctuations at the end of the Wisconsin Episode, Michigan, USA, in: Ehlers, J., Gibbard, P.L., Hughes, P.D. (Eds.), *Quaternary Glaciations—Extent and Chronology: A Closer Look*, *Developments in Quaternary Science*, Vol. 15. Elsevier, Amsterdam, pp. 489–497.
- Lidberg, M., Johansson, J.M., Scherneck, H.-G., Milne, G.A., 2010. Recent results based on continuous GPS observations of the GIA process in Fennoscandia from BIFROST. *J. Geodyn.* 50 (1), 8–18.
- Lisitsyn, A.P., 2001. Heat and mass fluxes in the Earth's exterior and interior spheres, in: *Global Change [in Russian]*. Geo, Novosibirsk, pp. 163–248.
- Marshak, S., Larson, T.H., Abert, C.C., 2016. *Geological and Geophysical Maps of the Illinois Basin—Ozark Dome Region*. Illinois State Geological Survey, University of Illinois.
- Maupin, V., Agostini, A., Artemieva, I., Balling, N., Beekman, F., Ebbing, J., England, R.W., Frassetto, A., Gradmann, S., Jacobsen, B.H., Köhler, A., Kvarven, T., Medhus, A.B., Mjelde, R., Ritter, J., Sokoutis, D., Stratford, W., Thybo, H., Wawerzinek, B., Weidle, C., 2013. The deep structure of the Scandes and its relation to tectonic history and present-day topography. *Tectonophysics* 602, 15–37.
- Mickelson, D.M., McCartney, M.C., 1979. *Glacial Geology of Dane County, Wisconsin, Scale 1:100000*. University of Wisconsin—Extension Geol. Natural History Survey.
- Milne, G.A., Davis, J.L., Mitrovica, J.X., Scherneck, H.G., Johansson, J.M., Vermeer, M., Koivula, D., 2001. Space-geodetic constraints on glacial isostatic adjustment in Fennoscandia. *Science* 291 (5512), 2381–2385.
- Mitrofanov, F.P. (Ed.), 2012. *1:1000,000 Geological Map of the Kola Peninsula Region [in Russian]*. Kola Science Center, Apatity.
- Mooney, W.D., Kaban, M.K., 2010. The North American upper mantle: Density, composition, and evolution. *J. Geophys. Res.* 115 (B12424). DOI:10.1029/2010JB000866.
- Mörner, N.-A., 1969. The Late Quaternary history of the Kattegat Sea and the Swedish west coast: deglaciation, shorelevel displacement, chronology, isostasy and eustasy. *Sveriges Geol. Unders.* C-640, 1–487.
- Mörner, N.-A., 1980. The Fennoscandian uplift: geological data and their geodynamical implication, in: Mörner, N.A. (Ed.), *Earth: Phenology, Isostasy, Eustasy*. Wiley, London, pp. 251–284.
- Mörner, N.-A., 2004. Active faults and paleoseismicity in Fennoscandia, especially Sweden. Primary structures and secondary effects. *Tectonophysics* 380 (3–4), 139–157.
- Nikolaev, N.N. (Ed.), 1979. *1:5000,000 Neotectonic Map of the USSR and its Surroundings [in Russian]*. Nauka, Moscow.
- Nikolaeva, S.B., 2001. Record of past earthquakes in the southeast Fennoscandian shield. *Geomorfologiya*, No. 4, 66–74.
- Nikolaeva, S.B., Nikonov, A.A., Shvarev, S.V., Rodkin, M.V., 2018. Detailed paleoseismological research on the flank of the Lake Imandra depression (Kola region): New approaches and results. *Russian Geology and Geophysics (Geologiya i Geofizika)* 59 (6), 697–708 (866–880).
- Niskanen, E., 1939. On the upheaval of land in Fennoscandia. *Annu. Acad. Sci. Fennicae* 53 (10A), 1–30.
- Ojala, V.J., Kuivamäki, A., Vuorela, P., 2004. Postglacial deformation of bedrock in Finland. *Geol. Survey. Nucl., Waste Disp. Res., Rep. GTK-YST-120*, Finland.
- Olsen, O., 1988. The Stuaragurra Fault: evidence of neotectonics in the Precambrian of Finnmark, northern Norway. *Nor. Geol. Tidsskr.* 68, 107–118.
- Olesen, O., Lundin, E., Nordgulen, Ø., Osmundsen, P.T., Skilbrei, J.R., Smethurst, M.A., Solli, A., Bugge, T., Fichler, C., 2002. Bridging the gap between the onshore and offshore geology in Nordland, northern Norway. *Norw. J. Geol.* 82, 243–262.
- Panasenko, T.D., 1969. *Seismic Features of the Northeastern Fennoscandian Shield [in Russian]*. Nauka, Leningrad.
- Petrov, O., Pubellier, M. (Eds.), 2018. *Tectonic Map of the Arctic. 1:10 000 000 Scale (first edition)*. Commission for the Geological Map of the World.
- Redfield, T.F., Osmundsen, P.T., 2015. Some remarks on the earthquakes of Fennoscandia: A conceptual seismological model drawn from the perspective of hyperextension. *Norw. J. Geol.* 94, 233–262.
- Siegert, M.J., Dowdeswell, J., Melles, M., 1999. Late Weichselian glaciation of the Russian High Arctic. *Quat. Res.* 52 (3), 273–285.
- Siegert, M.J., Dowdeswell, J.A., Hald, M., Svendsen, J.I., 2001. Modelling the Eurasian Ice Sheet through a full (Weichselian) glacial cycle. *Global Planet. Change* 31 (1–4), 367–385.
- Simon, K.M., Riva, R.E.M., Kleinherenbrink, M., Frederikse T., 2018. The glacial isostatic adjustment signal at present day in northern Europe and the British Isles estimated from geodetic observations and geophysical models. *Solid Earth* 9 (3), 777–795.
- Stewart, I.S., Sauber, J., Rose, J., 2000. Glacio-seismotectonics ice sheets, crustal deformation and seismicity. *Quat. Sci. Rev.* 19 (14–15), 1367–1389.
- Svendsen, J.I., Alexanderson, H., Astakhov, V.I., Demidov, I., Dowdeswell, J.A., Funder, S., Gataullin, V., Henriksen, M., Hjort, C., Houmark-Nielsen, M., Hubberten, H.W., Ingólfsson, Ó., Jakobsson, M., Kjær, K.H., Larsen, E., Lokrantz, H., Lunkka, J.P., Lyså, A., Mangerud, J., Matiouchkov, A., Murray, A., Möller, P., Niessen, F., Nikolskaya, O., Polyak, L., Saarnisto, M., Siegert, C., Siegert, M.J., Spielhagen, R., Stein, R., 2004. Late Quaternary ice sheet history of northern Eurasia. *Quat. Sci. Rev.* 23 (11–13) 1229–1271.
- Syverson, K.M., Colgan, P.M., 2011. The Quaternary of Wisconsin: An updated review of stratigraphy, glacial history, and landforms, in: Ehlers, J., Gibbard, P.L., Hughes, P.D. (Eds.), *Quaternary Glaciations—Extent and Chronology: A Closer Look*, *Developments in Quaternary Science*, Vol. 15. Elsevier, Amsterdam, pp. 537–552.
- Tolkunova, T.L., 1977. Rheologic properties of the lithosphere according to data on recent crustal movements and the isostatic adjustment, in: *Earth Rheology and Late Cenozoic Isostatic Movement Symposium*. Geol. Inst., Stockholm, p. 127.
- Yanshin, A.L. (Ed.), 1966. *Tectonic Map of Eurasia [in Russian]*. Nauka, Moscow.
- Zharkov, V.N., 1983. *The Interior of the Earth and Planets [in Russian]*. Nauka, Moscow.